US007796726B1

(12) **United States Patent**
Gendreau et al.

(10) **Patent No.: US 7,796,726 B1**
(45) **Date of Patent: Sep. 14, 2010**

(54) **INSTRUMENT AND METHOD FOR X-RAY DIFFRACTION, FLUORESCENCE, AND CRYSTAL TEXTURE ANALYSIS WITHOUT SAMPLE PREPARATION**

(75) Inventors: **Keith Gendreau**, Greenbelt, MD (US); **Jose Vanderlei Martins**, Greenbelt, MD (US); **Zaven Arzoumanian**, Greenbelt, MD (US)

(73) Assignee: **University of Maryland, Baltimore County**, Baltimore, MD (US)

(*) Notice: Subject to any disclaimer, the term of this patent is extended or adjusted under 35 U.S.C. 154(b) by 302 days.

(21) Appl. No.: **11/706,693**

(22) Filed: **Feb. 14, 2007**

Related U.S. Application Data

(60) Provisional application No. 60/773,244, filed on Feb. 14, 2006, provisional application No. 60/776,576, filed on Feb. 24, 2006.

(51) **Int. Cl.**
G01N 23/223 (2006.01)
G01N 23/20 (2006.01)

(52) **U.S. Cl.** **378/46**; 378/44; 378/45; 378/49; 378/71; 378/76; 378/79; 378/80; 378/81; 378/82; 378/83

(58) **Field of Classification Search** 378/44, 378/45, 46, 49, 70, 71, 72, 73, 75, 76, 79, 378/80, 81, 82, 83
See application file for complete search history.

(56) **References Cited**

U.S. PATENT DOCUMENTS

5,491,738	A	2/1996	Blake et al.	378/71
5,832,054	A *	11/1998	Kuwabara	378/45
5,978,442	A *	11/1999	Kuwabara	378/46
6,163,592	A *	12/2000	He et al.	378/71
6,173,037	B1 *	1/2001	Brouwer	378/45
6,233,307	B1 *	5/2001	Golenhofen	378/45
6,295,333	B1 *	9/2001	Tamura	378/44
6,359,962	B1 *	3/2002	Yagi	378/44
6,370,220	B1 *	4/2002	Stoop	378/45
6,400,795	B2 *	6/2002	Yagi	378/45
6,577,705	B1 *	6/2003	Chang et al.	378/45
6,661,876	B2 *	12/2003	Turner et al.	378/138
6,718,008	B1 *	4/2004	He et al.	378/71
6,751,287	B1 *	6/2004	Kalyon et al.	378/71
6,798,863	B2 *	9/2004	Sato	378/46
6,836,532	B2 *	12/2004	Durst et al.	378/73
7,245,696	B2 *	7/2007	Yun et al.	378/45

(Continued)

OTHER PUBLICATIONS

B. D. Cullity and S. R. Stock, Elements of X-Ray Diffraction, third edition (New Jersey: Prentice-Hall, 2001), p. 216-217.*

Primary Examiner—Allen C. Ho
(74) *Attorney, Agent, or Firm*—Nixon Peabody LLP

(57) **ABSTRACT**

An X-ray diffraction and X-ray fluorescence instrument for analyzing samples having no sample preparation includes a X-ray source configured to output a collimated X-ray beam comprising a continuum spectrum of X-rays to a predetermined coordinate and a photon-counting X-ray imaging spectrometer disposed to receive X-rays output from an unprepared sample disposed at the predetermined coordinate upon exposure of the unprepared sample to the collimated X-ray beam. The X-ray source and the photon-counting X-ray imaging spectrometer are arranged in a reflection geometry relative to the predetermined coordinate.

15 Claims, 22 Drawing Sheets
(8 of 22 Drawing Sheet(s) Filed in Color)

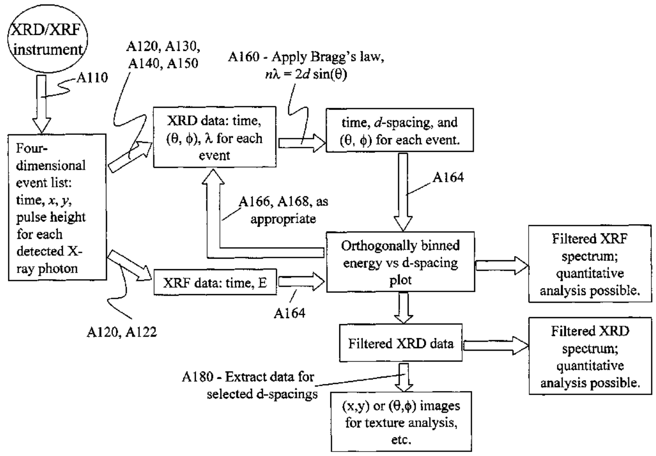

U.S. PATENT DOCUMENTS

7,321,652 B2 * 1/2008 Yokhin et al. 378/82
7,430,273 B2 * 9/2008 Yellepeddi 378/44
7,443,951 B2 * 10/2008 Kenning et al. 378/44

* cited by examiner

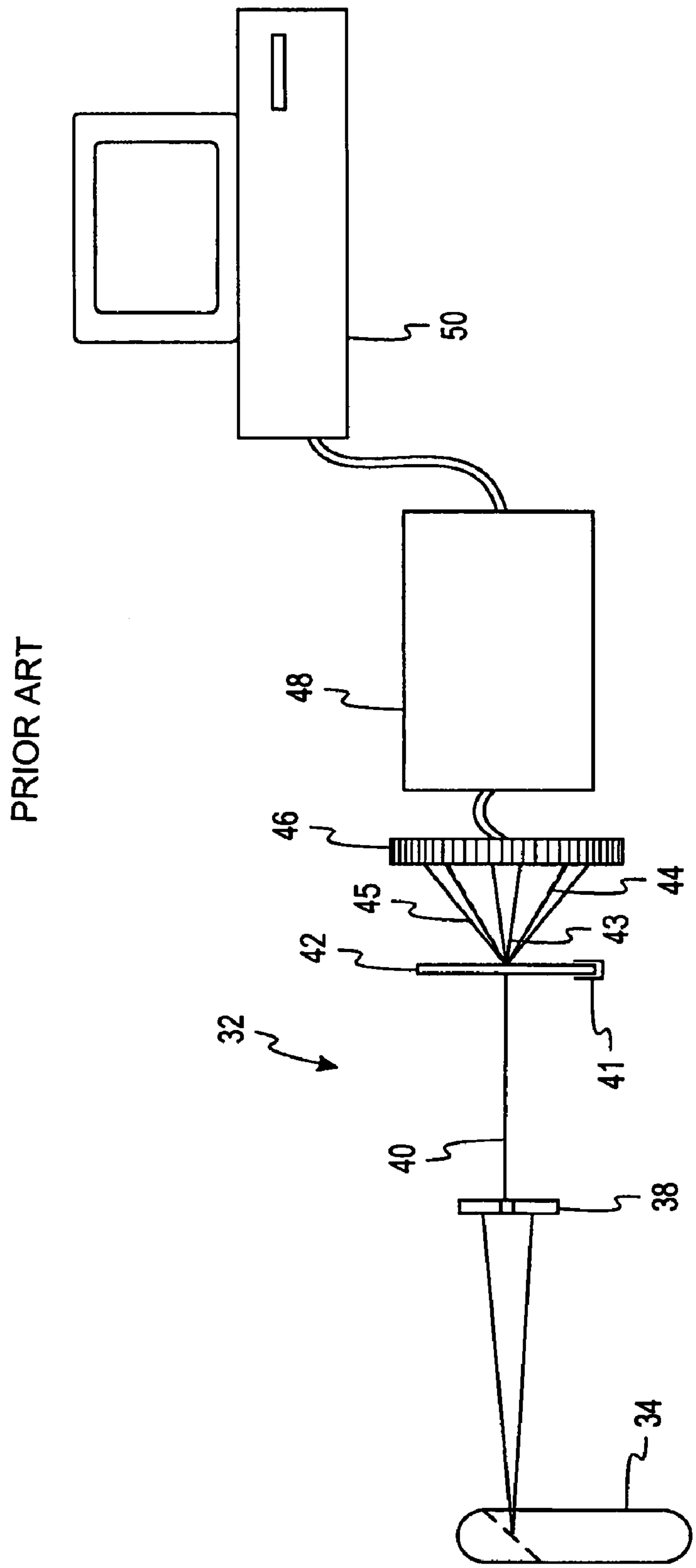

Fig. 1

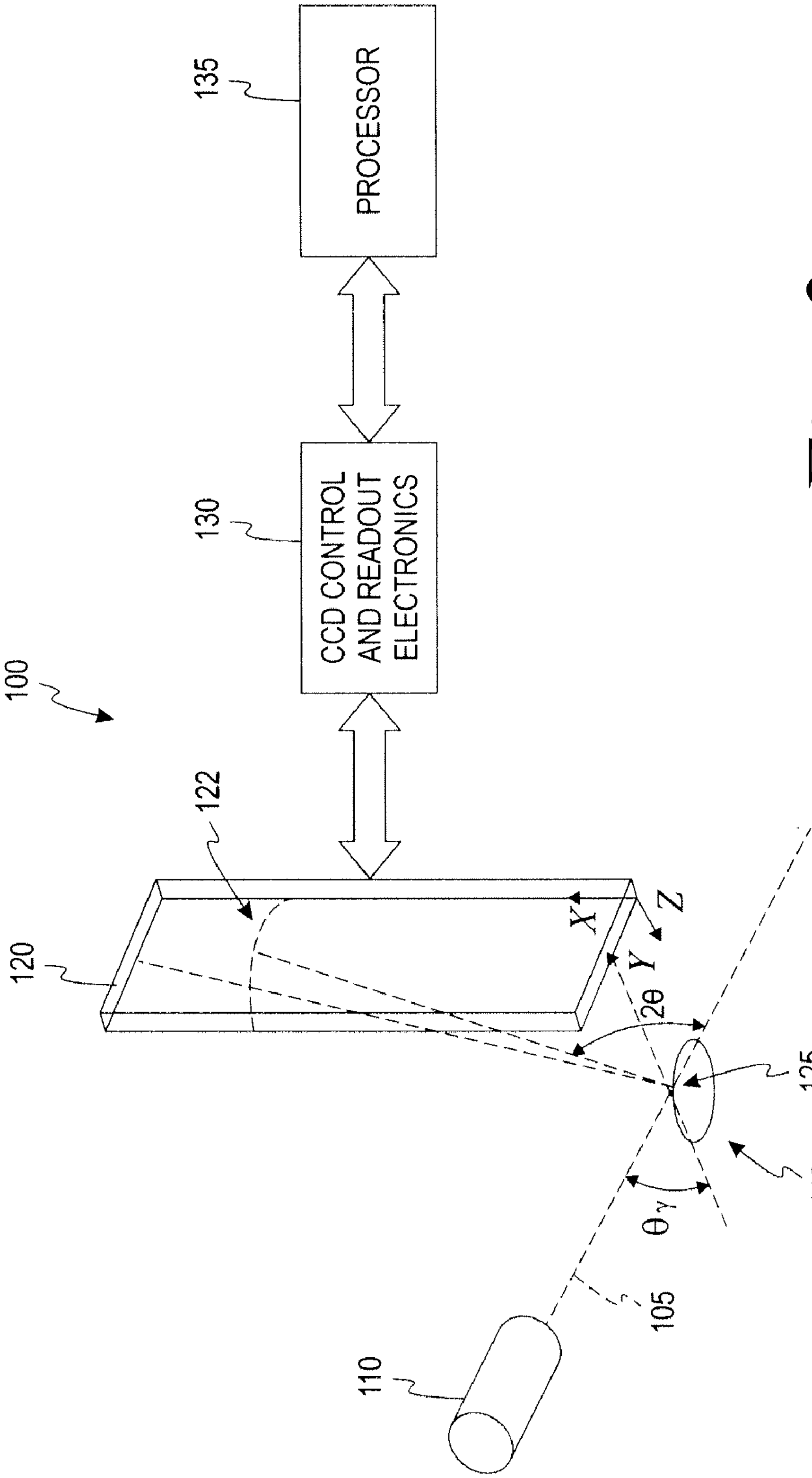
135
PROCESSOR
130
CCD CONTROL AND READOUT ELECTRONICS
100
120
122
X
Y
Z
2θ
125
(x_0, y_0, z_0)
140
θ_γ
105
110

Fig. 2a

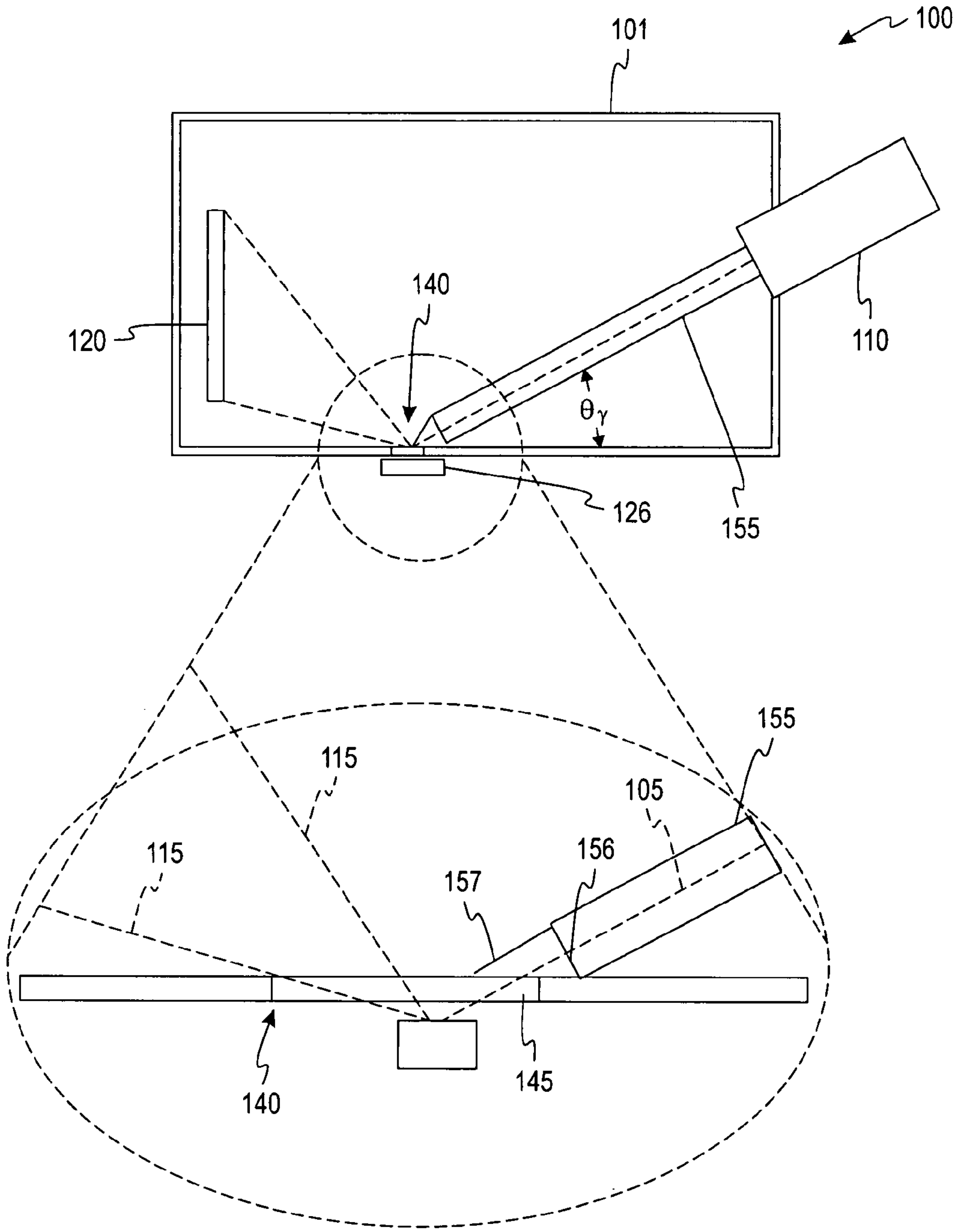
100
101
140
120
110
θ_γ
126
155
155
115
105
115
156
157
140
145

Fig. 2b

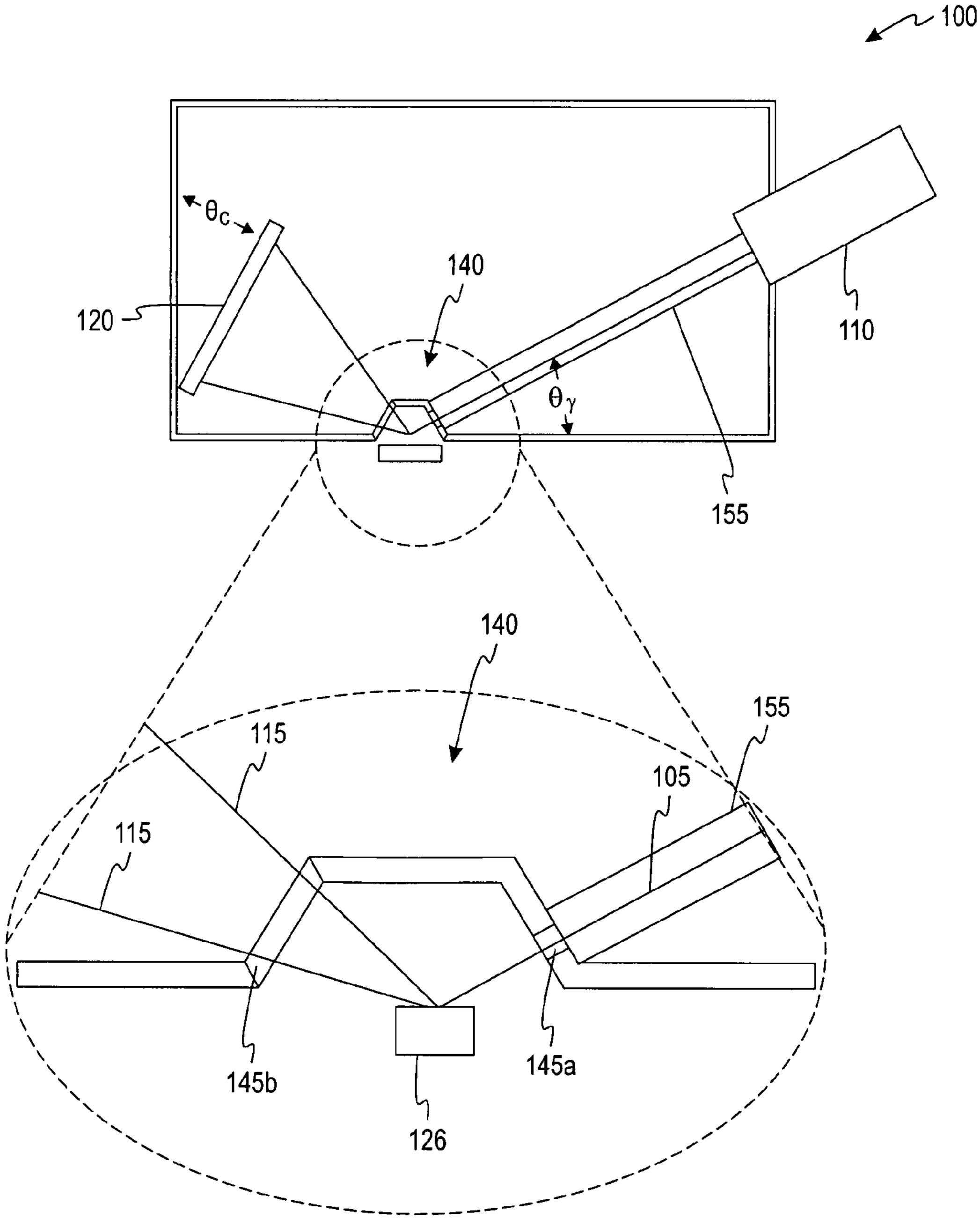
100
θ_c
140
120
110
θ_γ
155
140
115
155
105
115
145b
126
145a

Fig. 2c

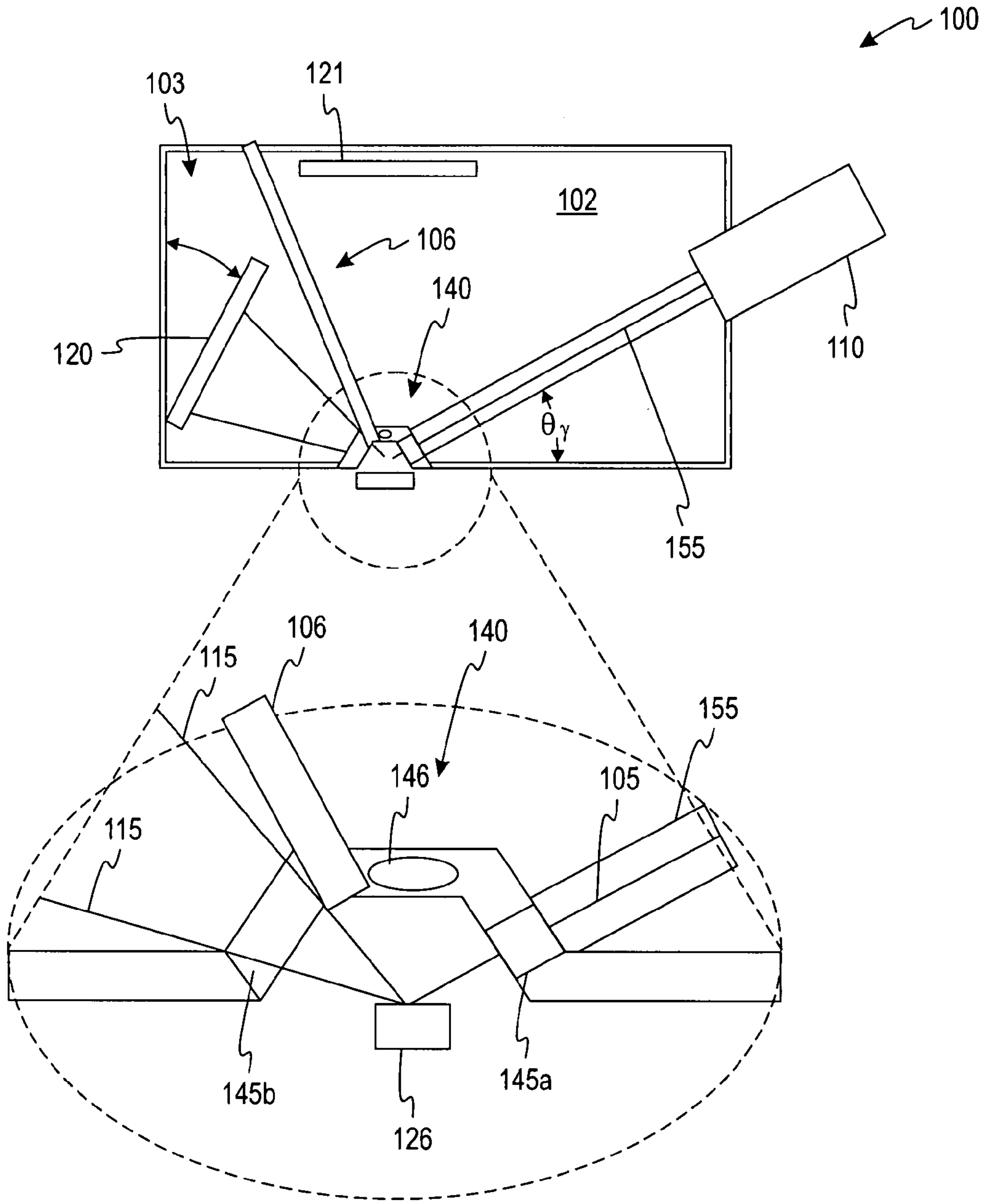
100
103
121
102
106
140
120
110
θ_{γ}
155
115
106
140
155
146
105
115
145b
145a
126

Fig. 2d

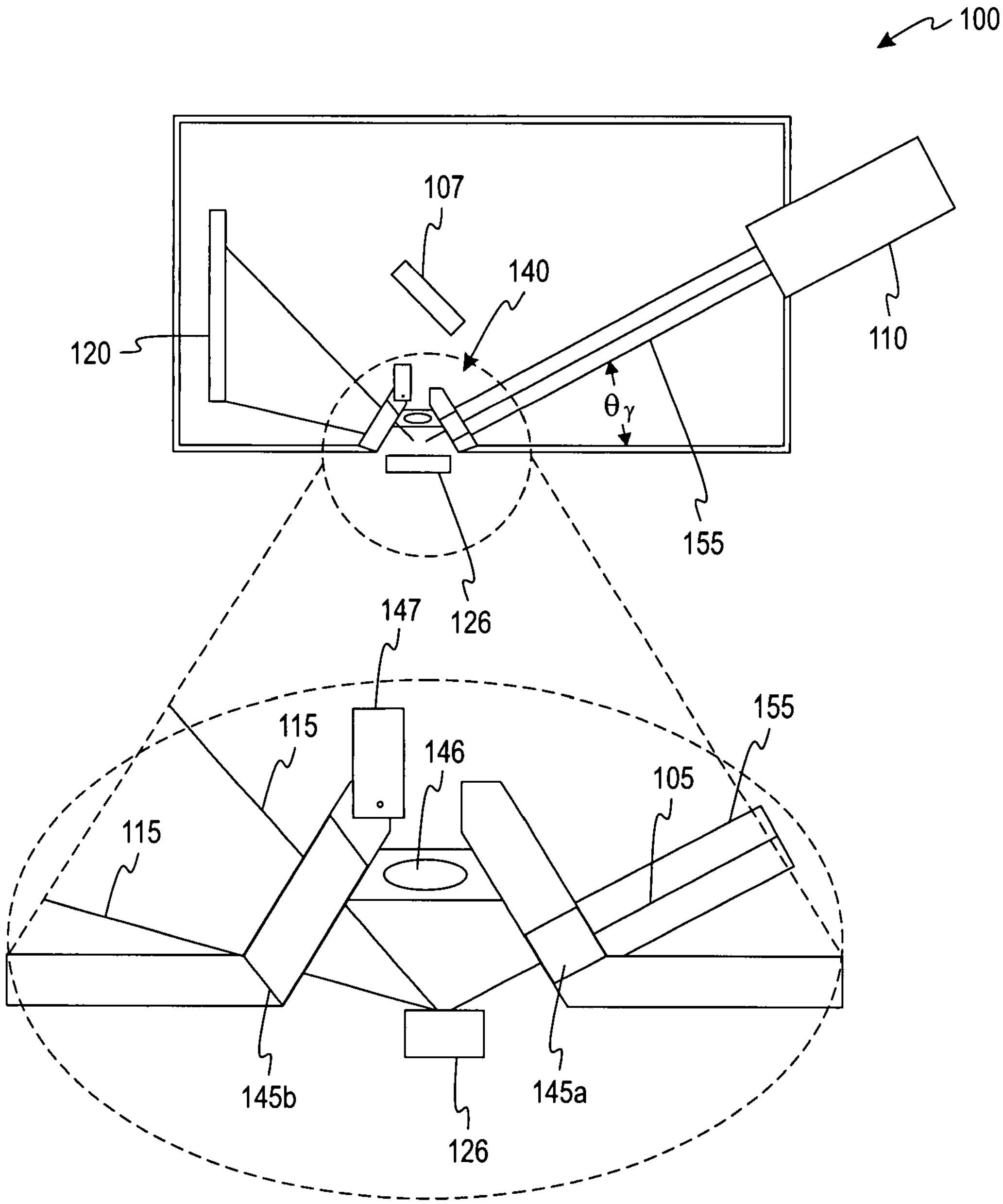
100
107
140
120
110
θ_γ
155
126
147
115
146
155
105
115
145b
145a
126

Fig. 2e

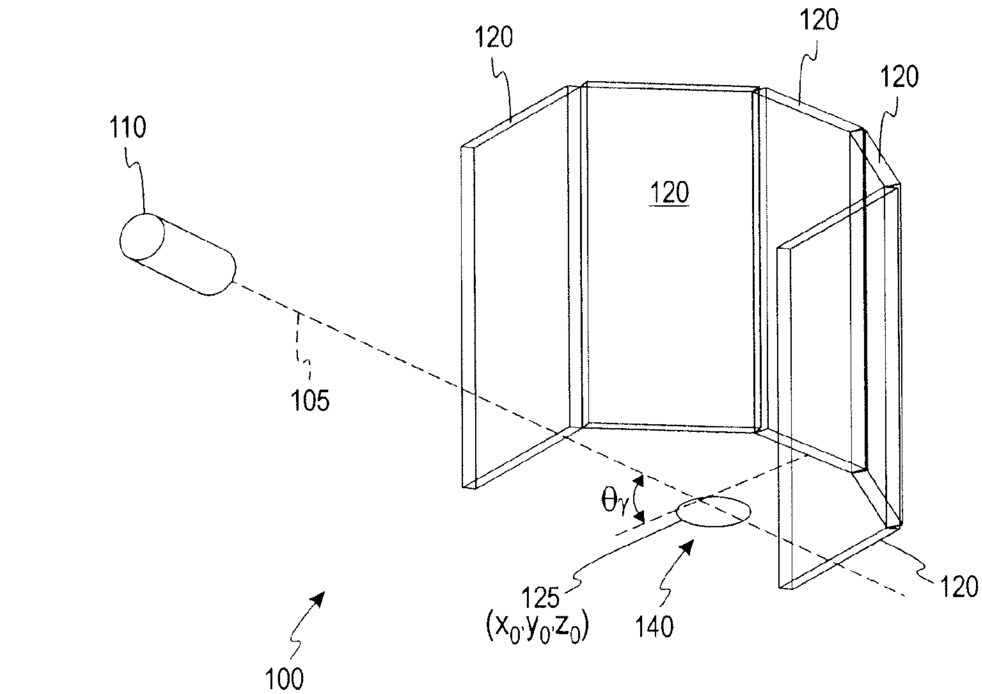
120
120
120
110
120
105
θ_Y
125
(x_0, y_0, z_0)
140
120
100

Fig. 3

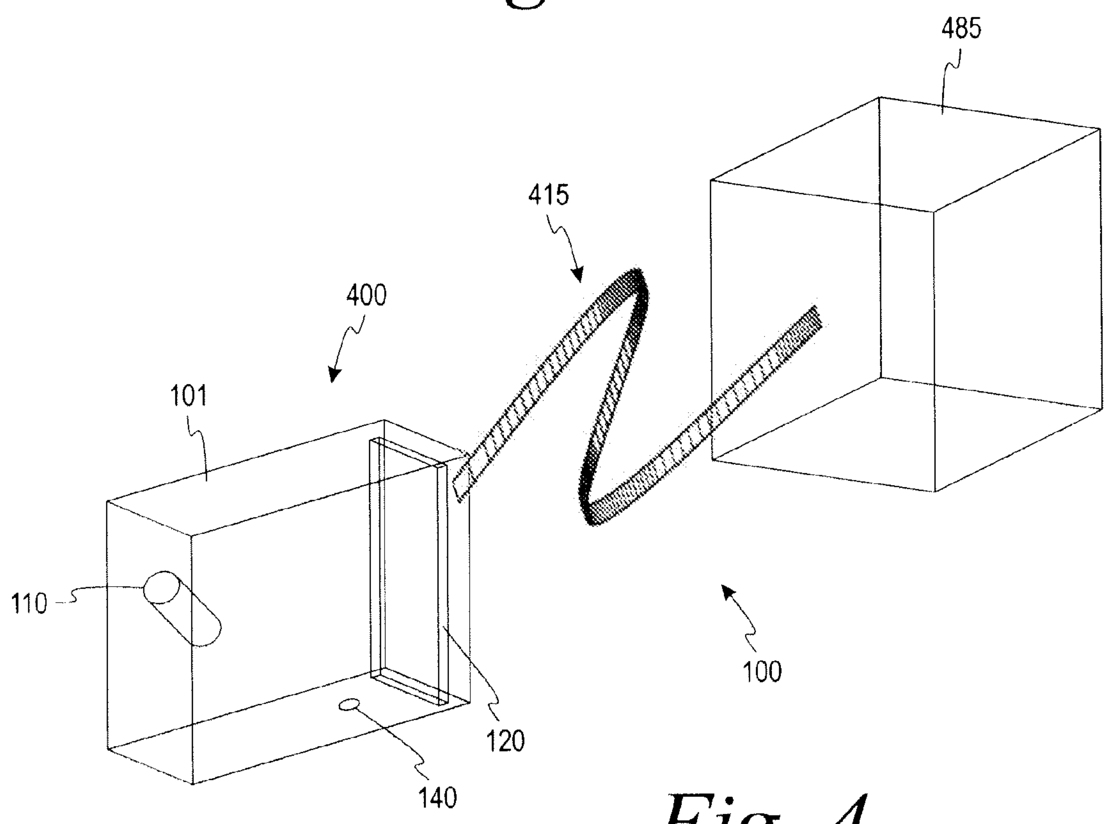
485
415
400
101
110
100
120
140

Fig. 4

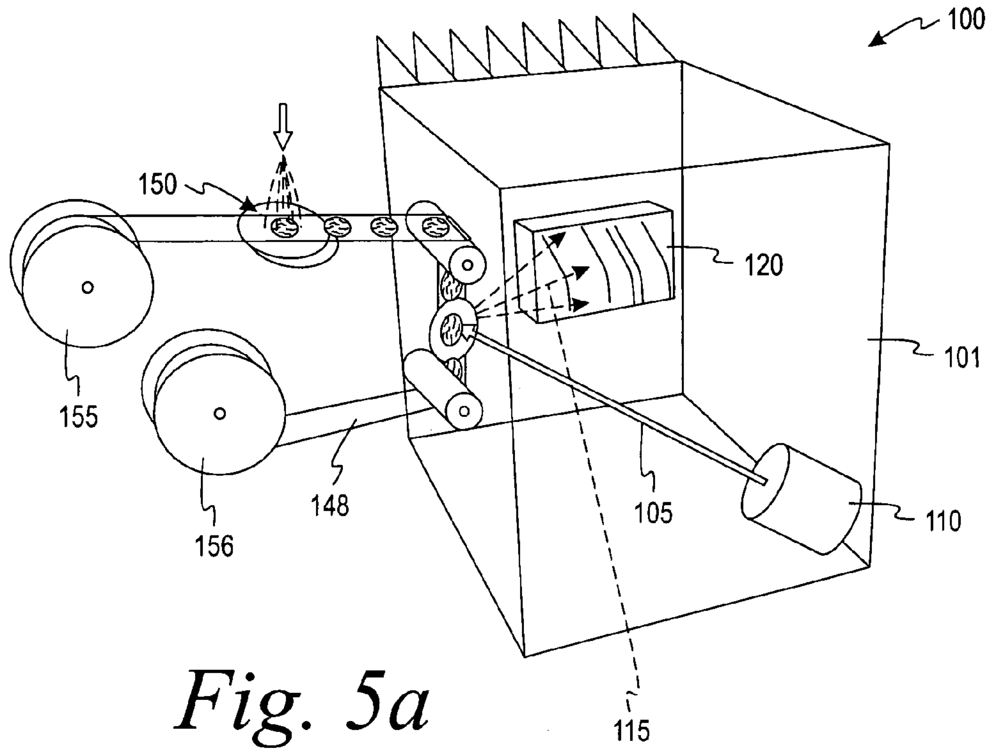
100
150
120
101
155
156
148
105
110
115

Fig. 5a

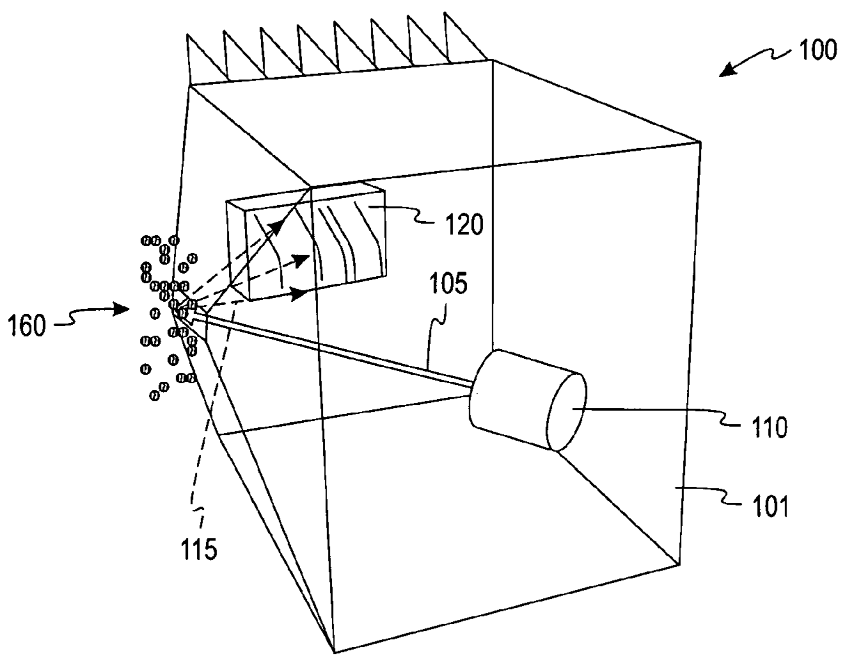
100
120
105
160
110
101
115

Fig. 5b

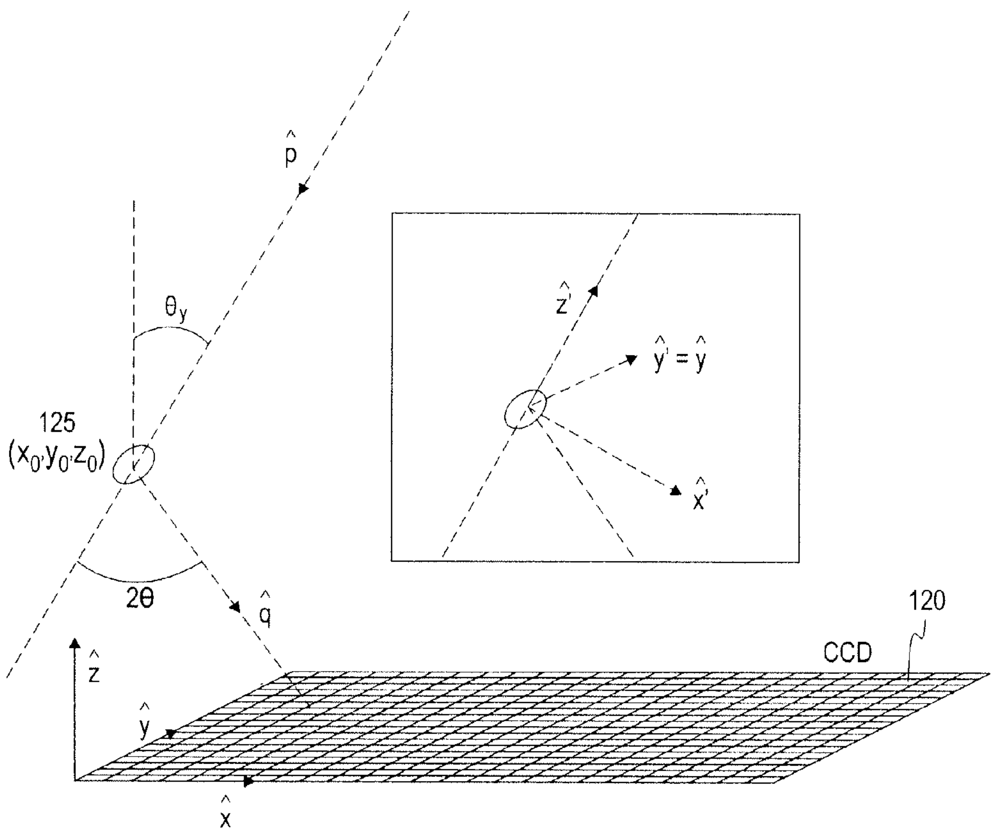

$\hat{p}$
θ_y
125
(x_0, y_0, z_0)
2θ
$\hat{q}$
$\hat{z}'$
$\hat{y}' = \hat{y}$
$\hat{x}'$
120
CCD
$\hat{z}$
$\hat{y}$
$\hat{x}$

Fig. 6

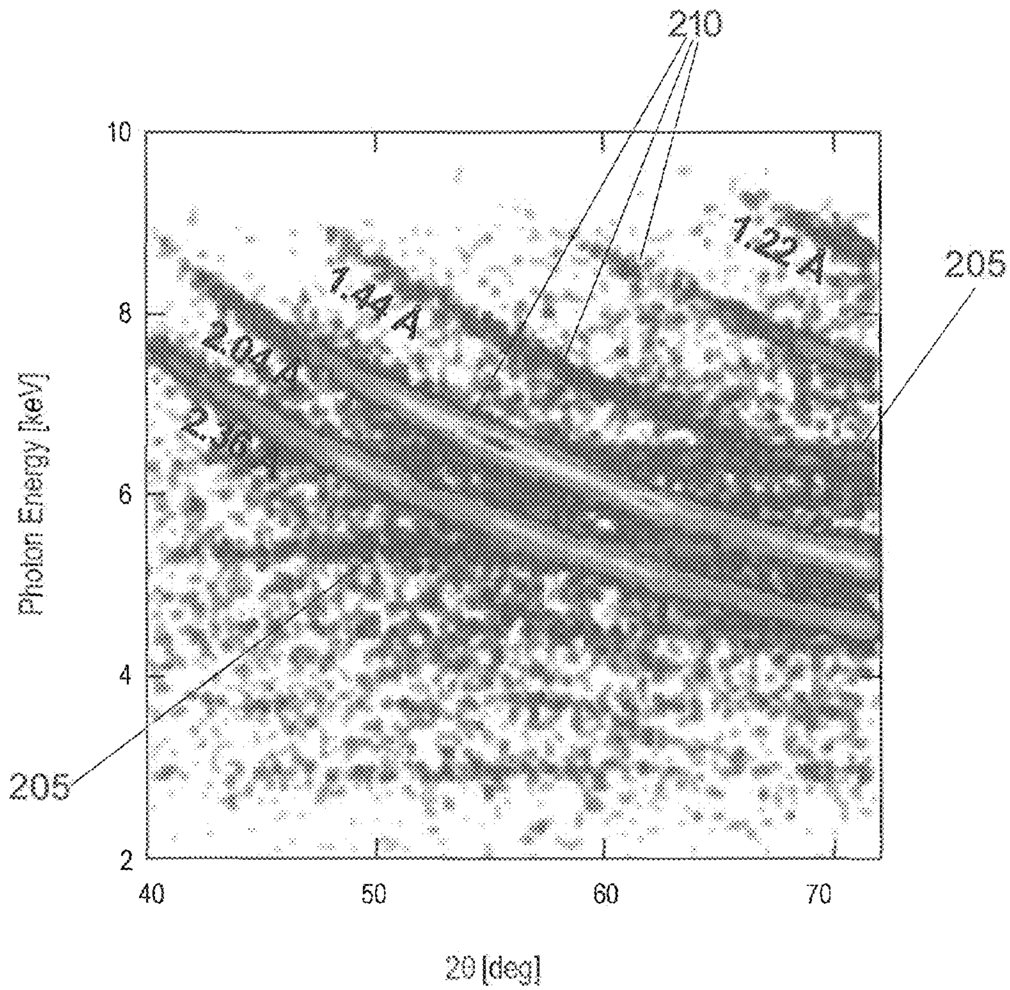
210
205
1.22 Å
1.44 Å
2.04 Å
10
8
6
4
2
40
50
60
70
Photon Energy [keV]
2θ [deg]

Fig. 7a

Fig. 7c

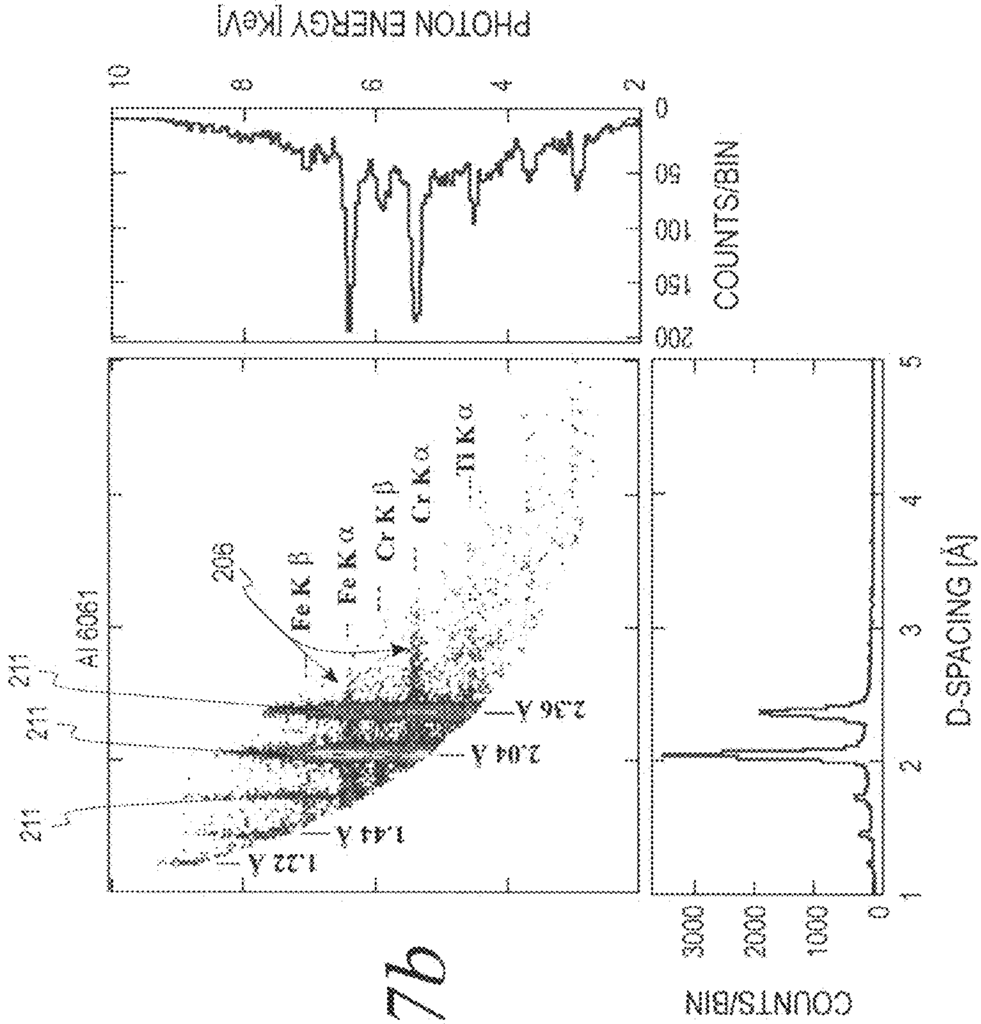

Fig. 7b

Fig. 7d

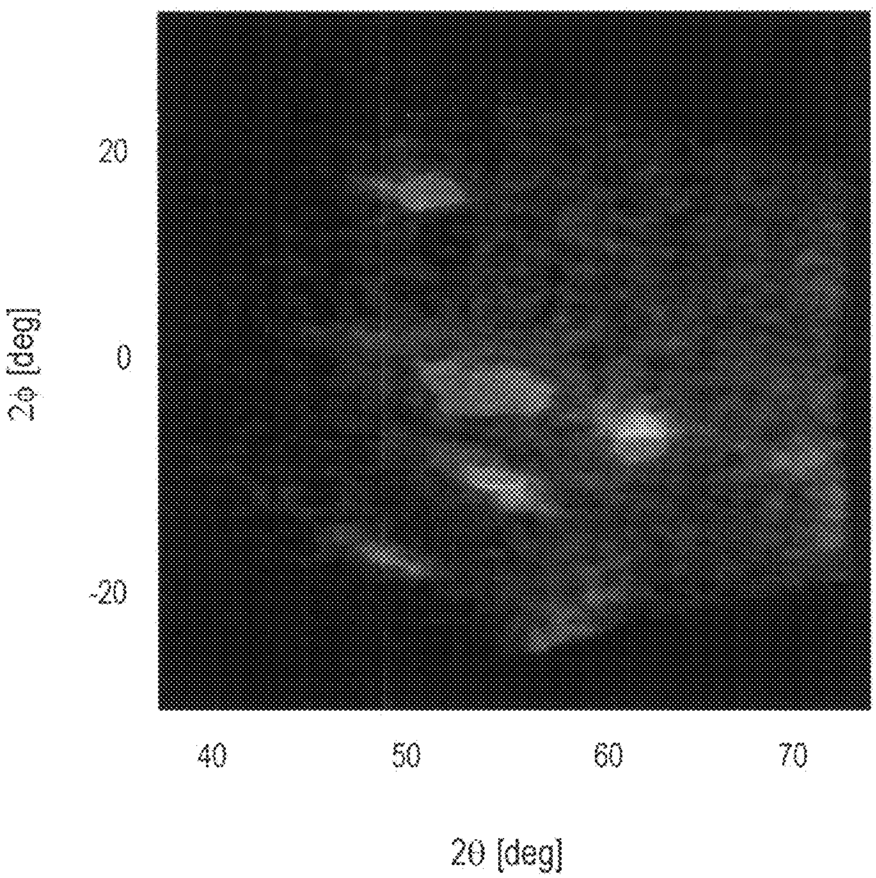

Fig. 7e

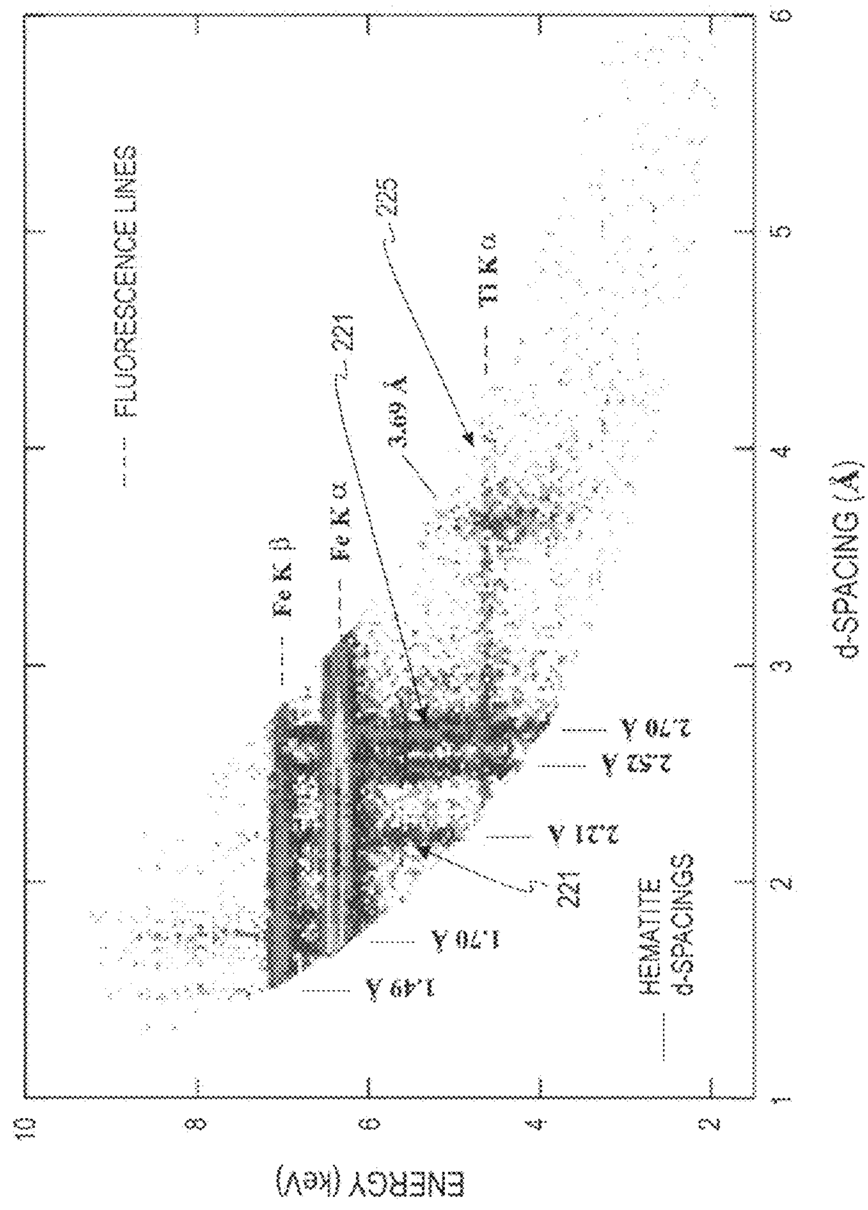
FLUORESCENCE LINES
HEMATITE
d-SPACINGS
Fe K β
Fe K α
Ti K α
3.69 Å
2.70 Å
2.52 Å
2.21 Å
1.70 Å
1.49 Å
221
221
225
ENERGY (keV)
d-SPACING (Å)
10
8
6
4
2
1
2
3
4
5
6

Fig. 8

Fig. 9c

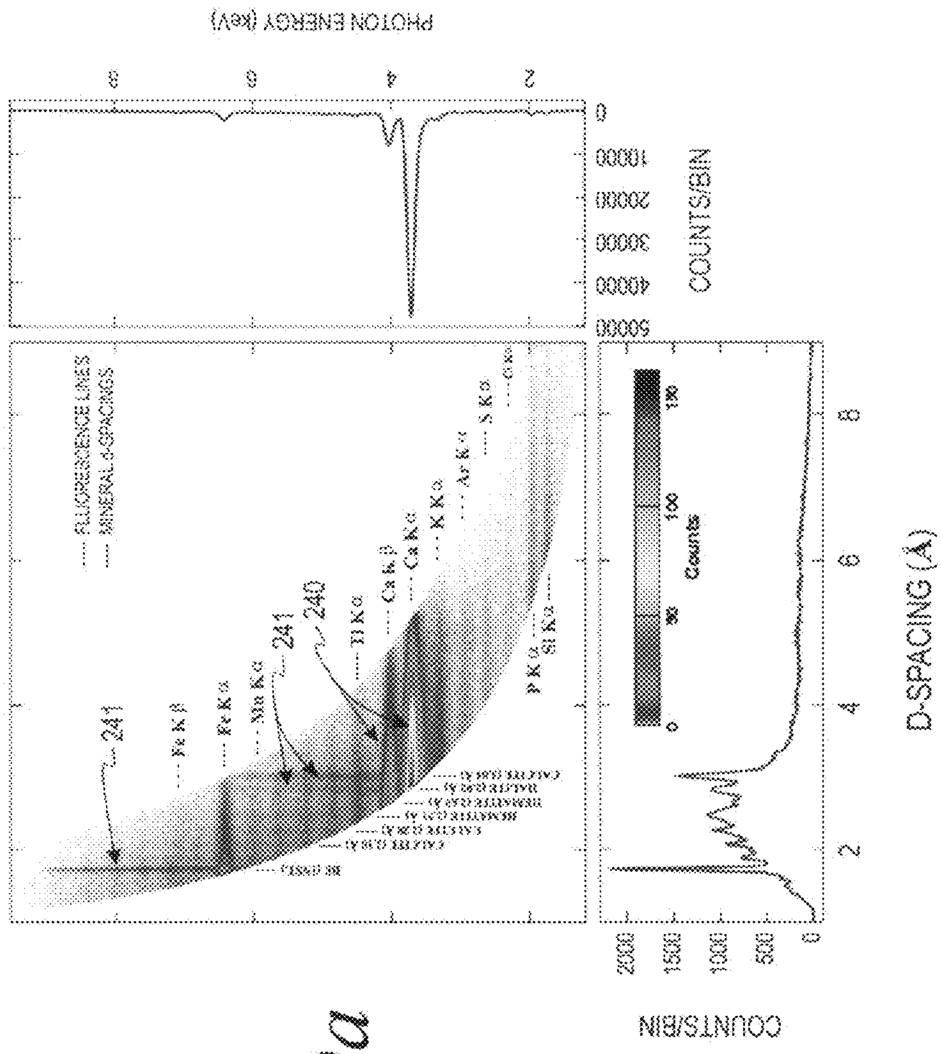

Fig. 9b

Fig. 9a

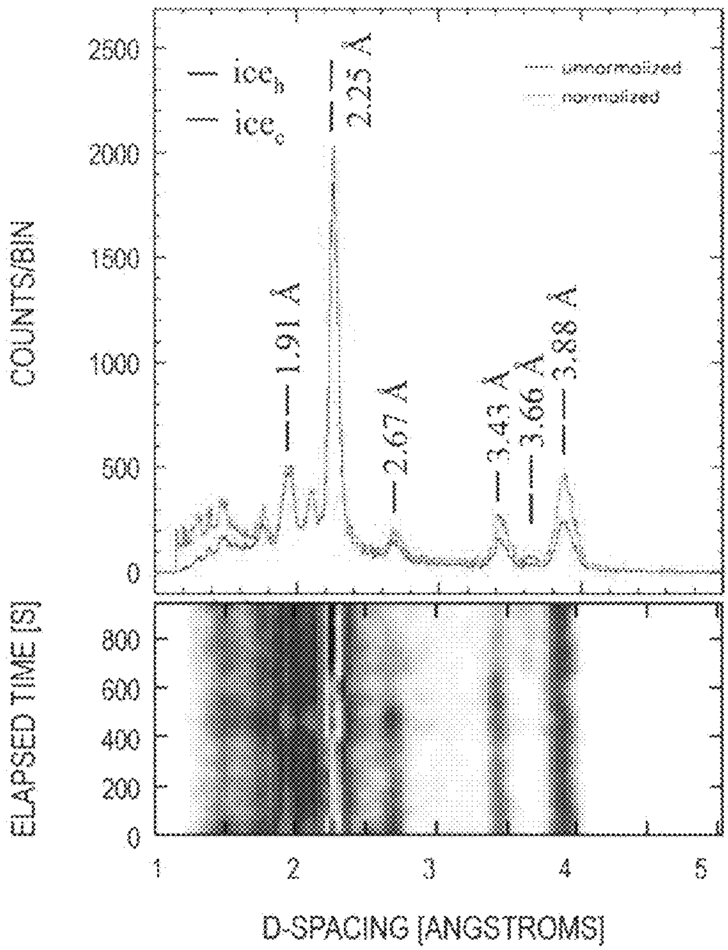

Fig. 10a

Fig. 10b

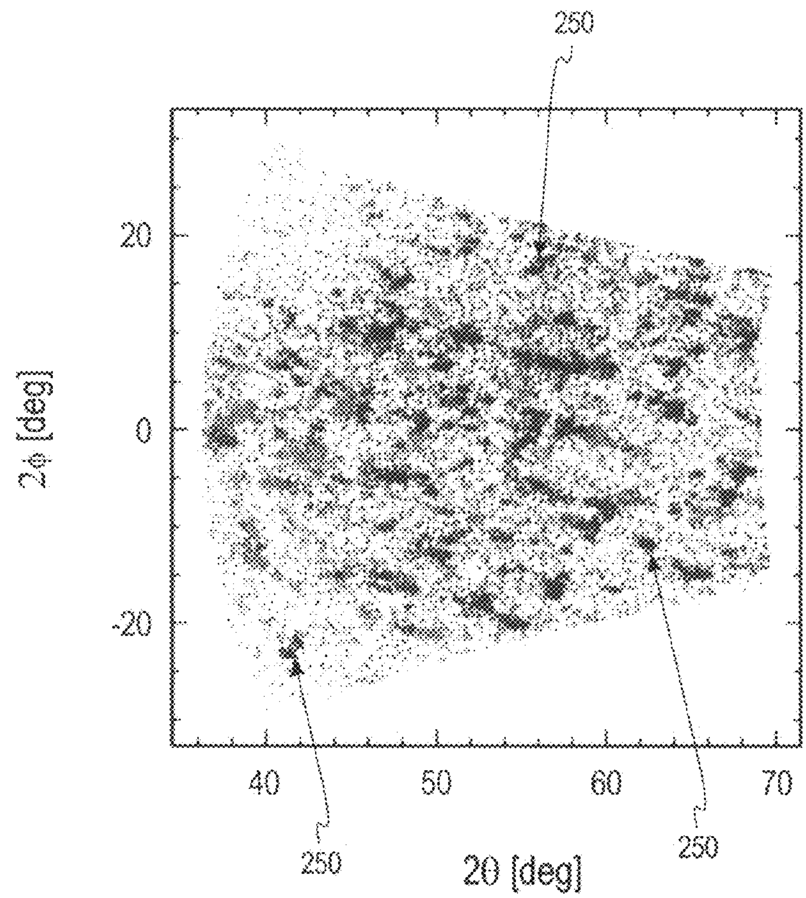

Fig. 10c

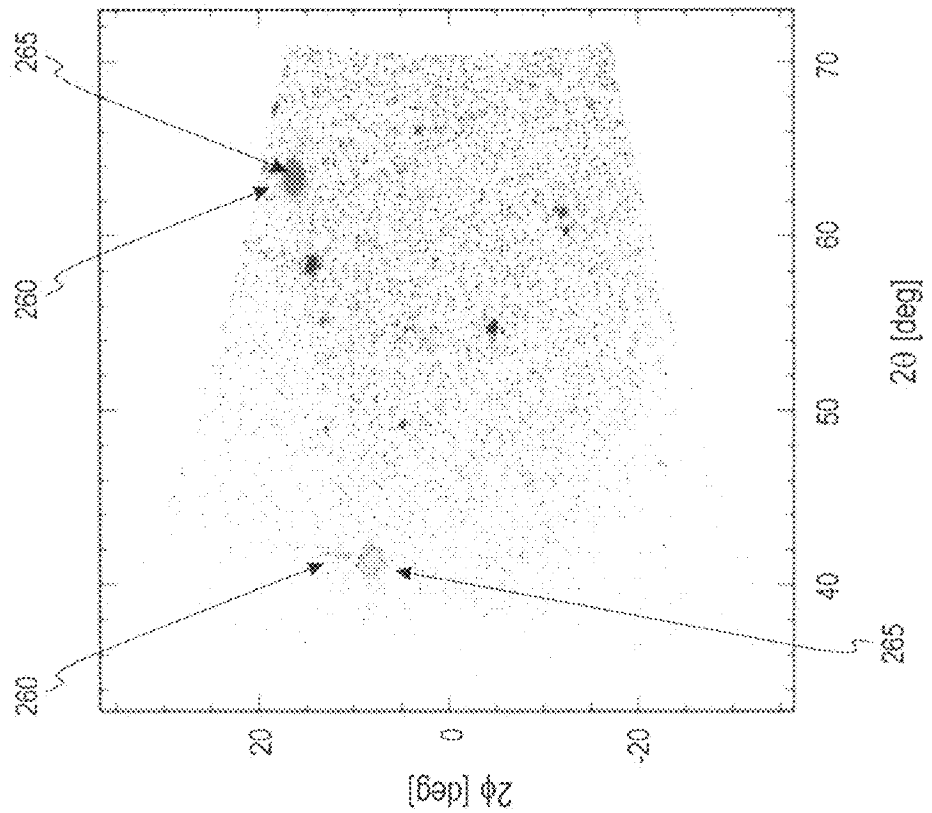

Fig. 11b

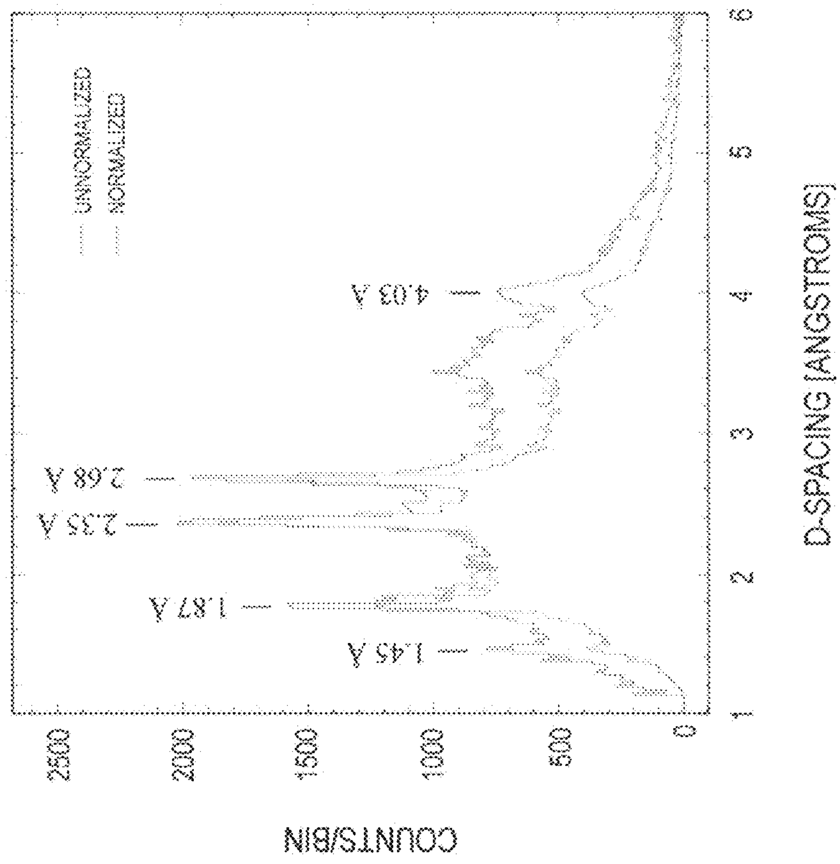

Fig. 11a

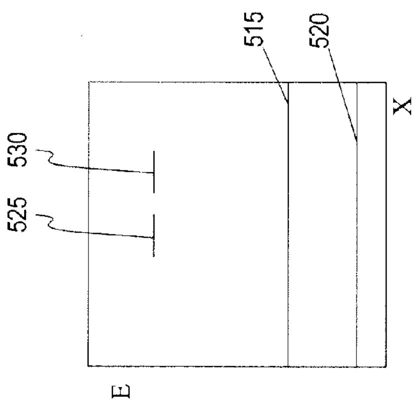

Fig. 12b

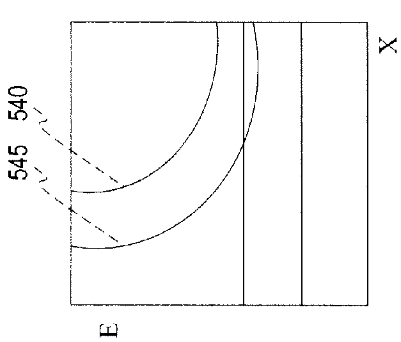

Fig. 13b

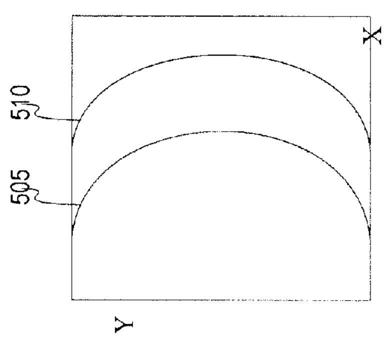

Fig. 12a

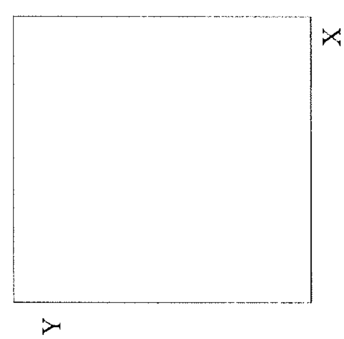

Fig. 13a

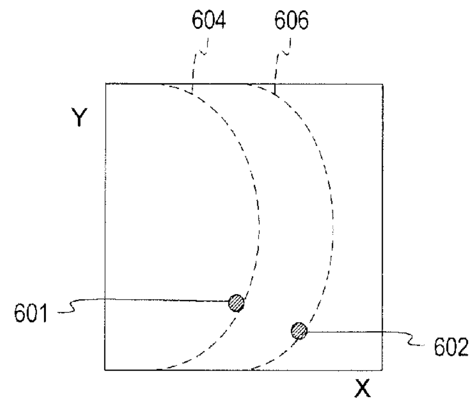

Fig. 14a

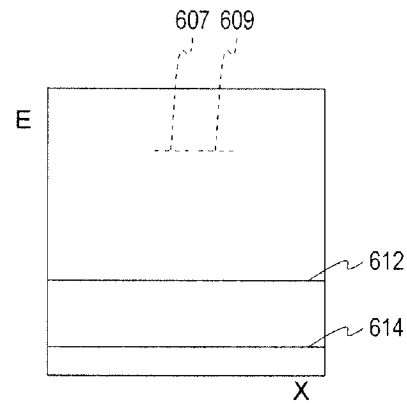

Fig. 14b

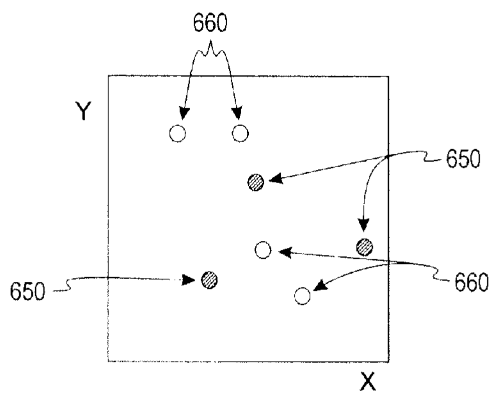

Fig. 15a

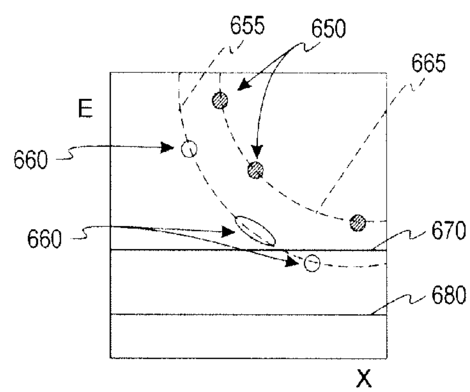

Fig. 15b

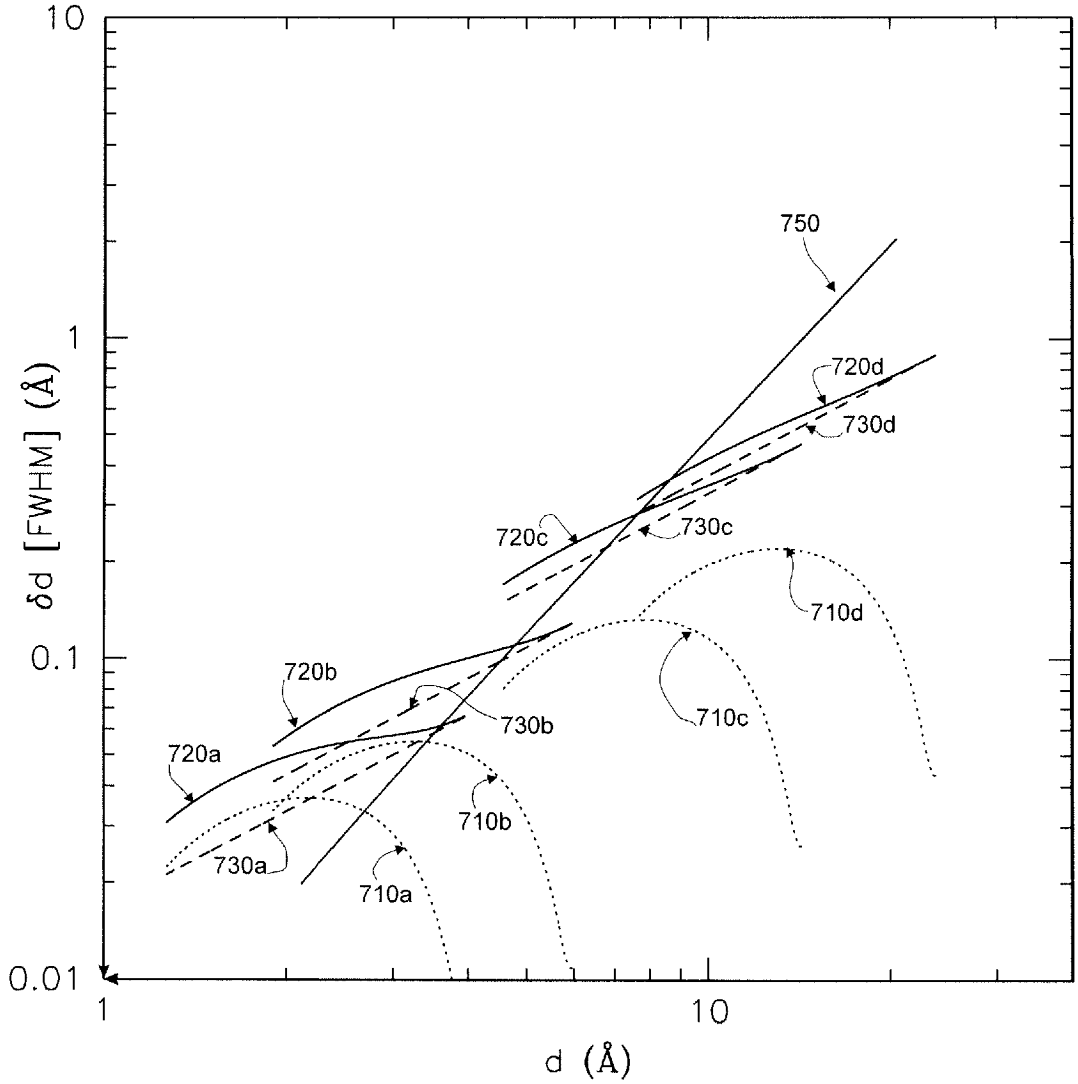
10
1
0.1
0.01
1
10
δd [FWHM] (Å)
d (Å)
750
720d
730d
720c
730c
710d
720b
730b
710c
720a
710b
730a
710a

Fig. 16

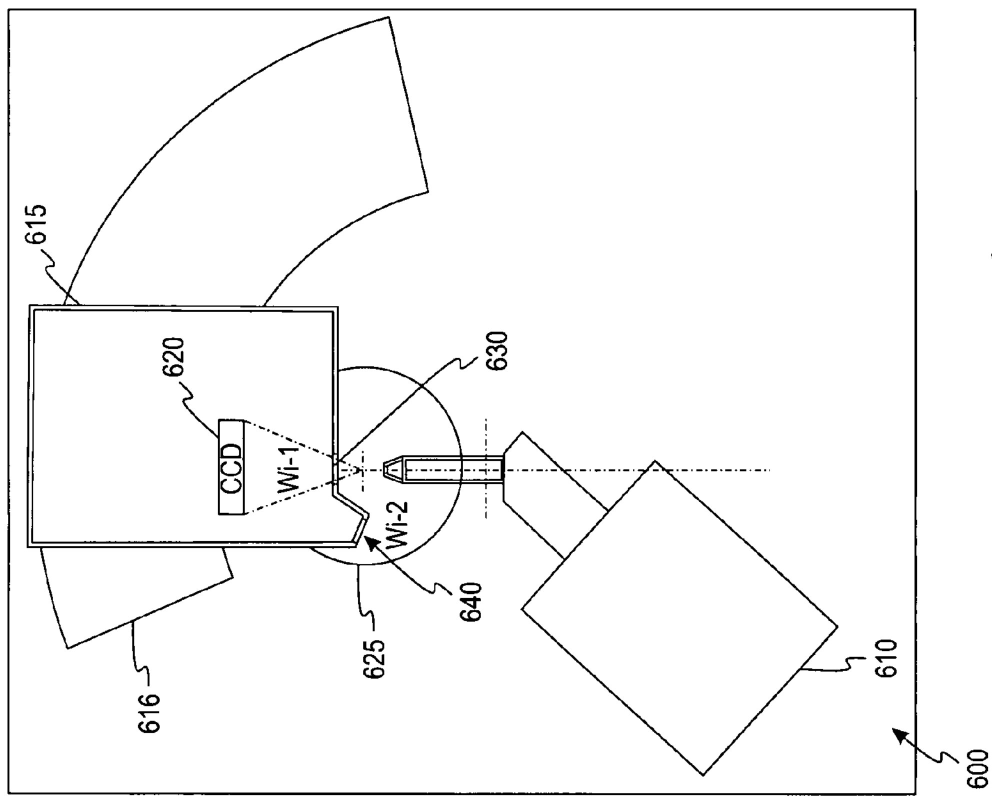

Fig. 17a

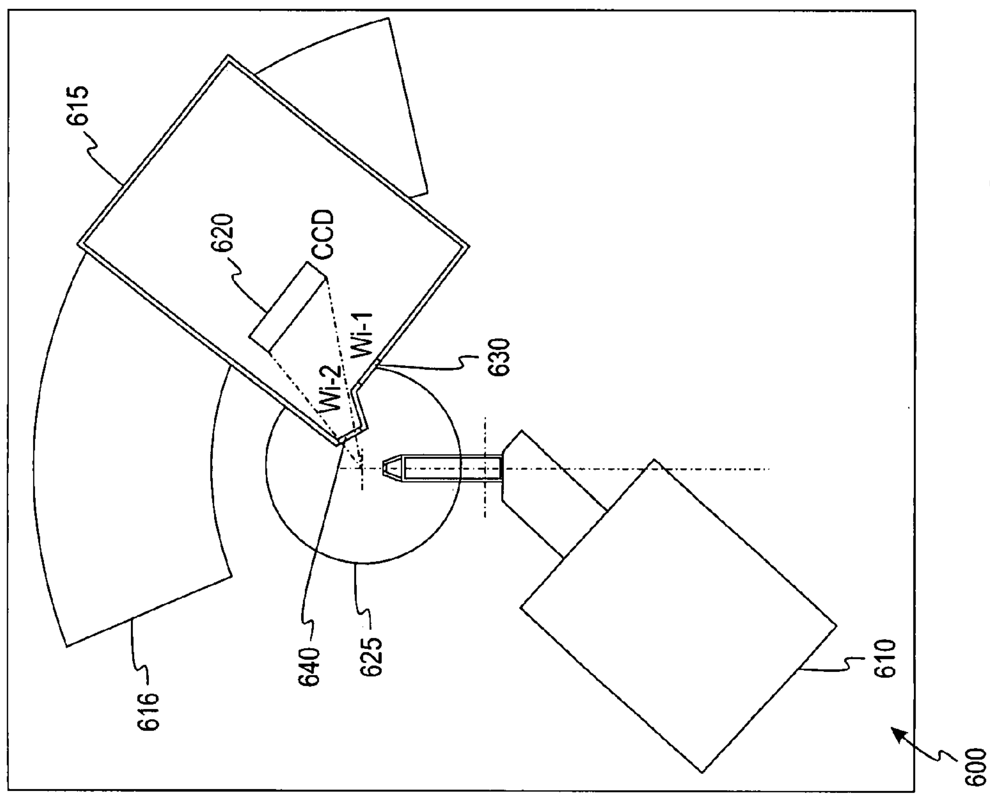

Fig. 17b

FIG. 18

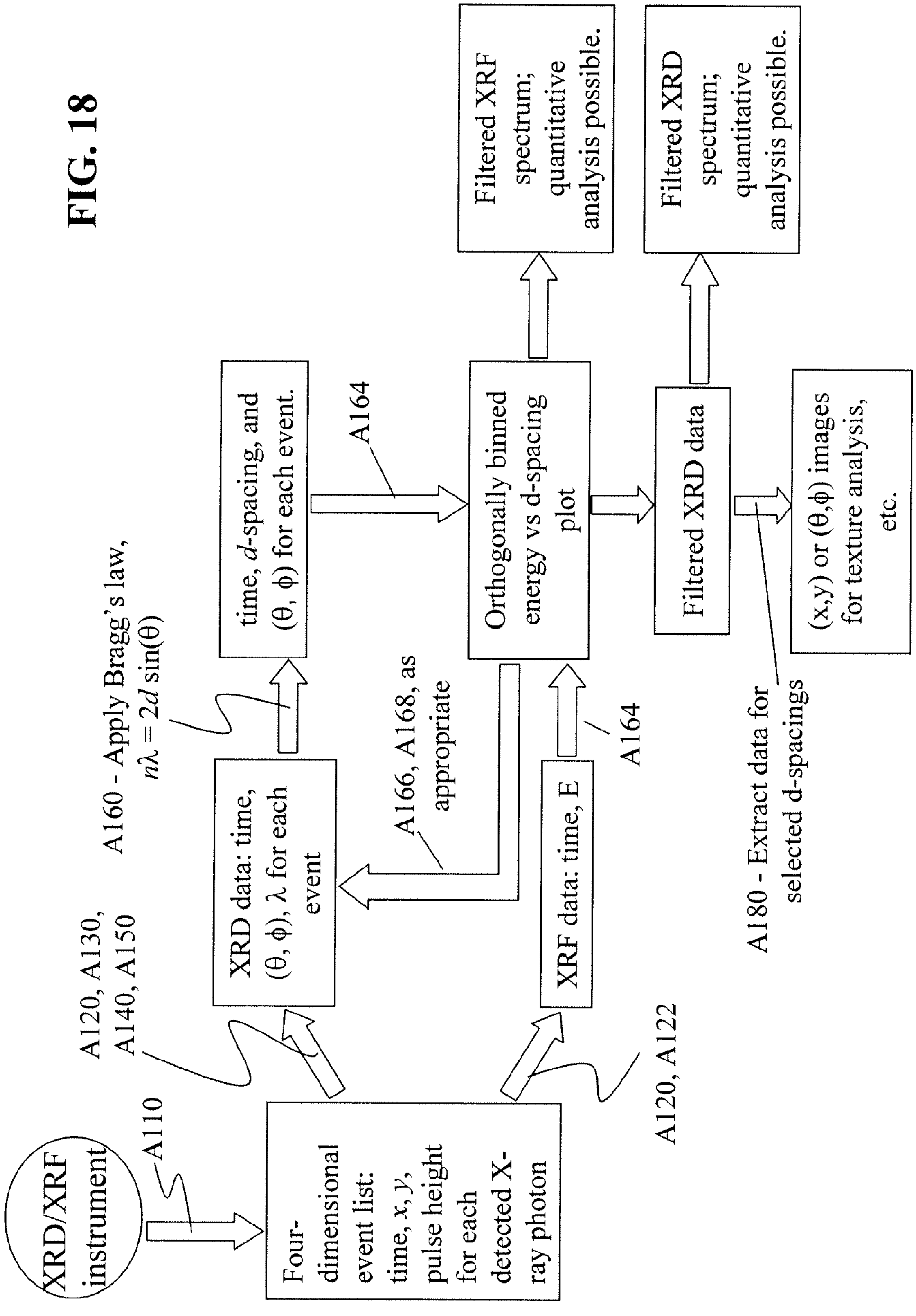
XRD/XRF instrument
A110
Four-dimensional event list: time, x, y, pulse height for each detected X-ray photon
A120, A130, A140, A150
A120, A122
XRD data: time, (θ, ϕ), λ for each event
XRF data: time, E
A160 - Apply Bragg's law, $n\lambda = 2d\sin(\theta)$
time, d-spacing, and (θ, ϕ) for each event.
A166, A168, as appropriate
A164
A164
Orthogonally binned energy vs d-spacing plot
Filtered XRF spectrum; quantitative analysis possible.
Filtered XRD spectrum; quantitative analysis possible.
Filtered XRD data
(x,y) or (θ,ϕ) images for texture analysis, etc.
A180 - Extract data for selected d-spacings

INSTRUMENT AND METHOD FOR X-RAY DIFFRACTION, FLUORESCENCE, AND CRYSTAL TEXTURE ANALYSIS WITHOUT SAMPLE PREPARATION

CROSS-REFERENCE TO RELATED APPLICATION

This application claims the benefit of the U.S. Provisional Patent Application No. 60/773,244 filed on Feb. 14, 2006 and entitled "Instrument And Method For X-ray Diffraction, Fluorescence, And Crystal Texture Analysis Without Sample Preparation" and U.S. Provisional Application No. 60/776,576 filed on Feb. 24, 2006 and entitled "Instrument And Method For X-ray Diffraction, Fluorescence, And Crystal Texture Analysis Without Sample Preparation" and each of these provisional patent applications is hereby incorporated by reference in its entirety.

RELATED APPLICATIONS

The invention described herein was made in the performance of work under a NASA contract or grant and by employees of the United States Government and is subject to the provisions of Section 305 of the National Aeronautics and Space Act of 1958, as amended, Public Law 85-568 (72 Stat. 435, 42 USC 2457) and may be manufactured and used by or for the Government for governmental purposes without the payment of any royalties thereon or therefor. The NASA grant numbers are NNG-05-CQ-79-A, NCC5-637 and RSP-0269-0154.

COPYRIGHT

FIELD OF THE INVENTION

The present concepts relate generally to X-ray diffraction and X-ray fluorescence devices and methods of analyses of material data produced thereby.

BACKGROUND OF THE INVENTION

It is often the case that various material samples need to be analyzed for (1) identification of elemental composition, molecular makeup, or mineral content, (2) study of crystallization (e.g., in the study of food shelf lives), (3) evidence of stress and shock, (4) crystallite size and orientation distributions (i.e., crystalline texture). X-ray diffraction (XRD) is one of the primary techniques used by mineralogists and solid state chemists to examine various physical and chemical properties of unknown solids.

FIG. **1** shows a schematic representation of one conventional x-ray diffraction/x-ray fluorescence (XRD/XRF) instrument designed to characterize elemental composition and mineralogy from small fine-grained or powdered samples. This XRD apparatus **32**, dubbed "CHEMIN" or "CheMin" due to its ability to provide a combined CHEmical and MINeralogical analysis, is disclosed in U.S. Pat. No. 5,491,738 to Blake et al. CheMin is one embodiment of the invention described in Blake et al.

The XRD apparatus **32** of FIG. **1** was designed to analyze x-ray diffraction pattern(s) from a thin-film sample **42** disposed in a sample holder **41**. The sample has a sample thickness that allows production of diffracted x-rays at the back side of the sample (e.g., a transmissive Laue method) when the thin-film sample **42** is irradiated with beam **40**. An x-ray emitter **34**, such as a CuK_a emitter, is used to produce a broad spectrum of x-ray energies in a non-collimated beam. The non-collimated beam is passed through a collimator **38** to produce a collimated beam **40**. The x-rays that are transmitted through the thin-film sample **42** are, in turn, incident upon a charge-coupled device (CCD) **46** containing a 2-dimensional planar array of pixels. The CCD **46** is an array detector adapted to record the energy of and position of individual incident X-rays.

Primary and secondary X-rays produced by irradiation of the sample **42** are directed onto the pixel array of the CCD **46**. FIG. **1** shows three different diffraction cones **43**, **44**, and **45**, which are due to diffraction from different-energy x-rays in the beam. A controller unit **48** is provided to receive input signals from each of the pixels in the CCD **46**, relating to the pixel position and photon energy measured at each pixel, for use in constructing the diffraction pattern of photons within a selected energy range striking the array. A microprocessor **50** is used to provide a screen display for the controller unit and to permit control of the CCD settings by a user.

During irradiation, only a small region (e.g., 50 μm in diameter) is illuminated by the collimated X-ray beam **40**. Following an exposure and data collection for a given substrate position, the thin-film sample **42** and/or x-ray emitter **34** is moved to a new position to expose another area of the thin-film sample **42**. The x-rays are diffracted from the planes of atoms in the thin-film sample **42** into a spatial pattern on the CCD **46** that reveals the distribution of atoms in the sample. The spatial pattern of the diffracted X-rays detected by the CCD **46** is analyzed using Bragg's Law, which relates the wavelength (λ) of the X-ray, the atomic plane separation (d) of the sample, the diffracted angle (2θ) of the X-ray away from its original course, and the diffraction order (n) by the equation $n*\lambda=2*d*\sin(\theta)$. For a fixed wavelength (λ), the detector must span a large enough angle (θ), so that atomic plane separations (d) can be determined.

In conventional XRD techniques, such as that described above, a sample of a material of interest is powdered and placed on a thin-film substrate, which is then disposed in a holder. The sample is typically ground to a powder (e.g., less than 10 μm to about 100 μm) using a mill or mortar and pestle or the like. In certain applications (e.g., laboratory), samples may be prepared using acetone, isopropanol, pentane, or the like to form a uniform slurry, so as to minimize any potential problem with preferred orientation which may accompany rod-like or plate-like crystals. The prepared sample is then positioned within the XRD instrument and illuminated with x-rays, typically of a fixed wavelength, and the intensity of the diffracted radiation is recorded. The sample and/or x-ray source is then repositioned. Ideally, a large number of crystallites in random orientations are exposed to the X-ray beam, which is typically done by moving the specimen in the beam to analyze a larger number of crystallites and/or larger number of orientations of crystallites. This data is then analyzed for the diffraction angle to calculate the inter-atomic spacing (D) and the intensity (I) is measured to discriminate (using I ratios) the various D spacings and the results are used to identify possible matches when compared to known values (e.g., "The International Tables for Crystallography", the "International Center for Diffraction Data®" (ICDD) Powder Diffraction File™ covering over 550,000 compounds, etc.).

In still other conventional techniques, in single-crystal XRD, a goniometer is used to rotate a single crystal so that many facets and sets of atomic planes are oriented so as to diffract monochromatic rays onto a fixed detector. A pattern of diffraction spots ("Laue spots") results which, through traditional crystallographic algorithms, may be inverted to determine the underlying geometric arrangement of the atoms in the crystal.

However, conventional XRD/XRF instruments require either significant sample preparation and/or require the ability to reposition the instrument through a wide range of angles around the sample, or rotate the sample through a wide range of angles, so as to get desired sample information (e.g., identification of elemental compositions, identification of molecular makeup, identification of mineral content, study of crystallization, evidence of stress and/or shock in the material, crystal grain size, crystal orientation distributions, etc.). In either case, several moving parts are required to perform the XRD analysis. However, in certain applications, such as extraterrestrial XRD analysis, the number of moving parts required increases (e.g., the CheMin device uses a carousel disc and associated drive system, sample preparation systems such as a fine-grinding mill, etc.), with corresponding increases in power consumption, mass, and risk. For the CheMin XRD/XRF apparatus **32**, which is presently slated for inclusion on the Mars Science Laboratory (MSL) mission scheduled for launch in 2009, sample preparation is required, which would disadvantageously destroy any water ice that MSL may encounter and cause it to evaporate in the low pressure environment on Mars. Sample preparation also destroys valuable scientific and engineering information regarding grain size and orientation distributions and evidence of stresses and shock.

SUMMARY OF THE INVENTION

In some aspects of the present concepts, an XRD/XRF instrument and method are provided which are particularly suited for extraterrestrial applications, such as may be used in combination with a rover, landing vehicle, or craft. Such a flight-instrument application requires that the instrument be robust, lightweight, and low in power consumption. In addition, risk must be minimized whenever possible. The XRD/XRF instrument presently disclosed herein, relative to conventional XRD/XRF instruments, eliminates moving parts, eliminates sample preparation needs, provides an efficient geometry, provides improved sensitivity, and eliminates the need to place samples in vacuum, each of which improvements decrease risk and, in combination, significantly decreases risks. Further, the XRD/XRF instrument and method provided herein should provide a platform for compact and rugged packaging that consumes a minimal amount of power. It is believed that a commercial XRD/XRF instrument based on the presently disclosed instrument and methods would cost significantly less than conventional XRD/XRF instruments.

In accord with disclosed aspects of the present concepts, an instrument and method for X-ray diffraction using a reflection geometry (and the methodology presented here; e.g. continuum X-ray source, and photon counting imaging spectrometer detectors) permit measuring the atomic plane spacings of unprepared material samples. The method described herein may alternatively be implemented in a transmission geometry. Further to providing material identification, the instrument(s) and method(s) permit the determination of the crystalline grain size, domain size, and orientation distributions (i.e., crystalline texture) within samples, which provide important information on crystallographic structure, material defects, and stresses or shocks that the sample may have experienced. The new method(s) described herein are very efficient compared to standard XRD techniques (including CheMin) for mineral and chemical identification. Further, the disclosed simultaneous X-ray fluorescence analysis capability provides elemental abundances.

According to one aspect of the present concepts an X-ray diffraction and X-ray fluorescence instrument for analyzing samples having no sample preparation includes a X-ray source configured to output a collimated X-ray beam comprising a continuum spectrum of X-rays to a predetermined coordinate and a photon-counting X-ray imaging spectrometer disposed to receive X-rays output from an unprepared sample disposed at the predetermined coordinate upon exposure of the unprepared sample to the collimated X-ray beam. The X-ray source and the photon-counting X-ray imaging spectrometer are arranged in a reflection geometry relative to the predetermined coordinate.

According to another aspect of the present concepts an X-ray diffraction and X-ray fluorescence instrument for analyzing samples, prepared or unprepared includes a X-ray source configured to output a collimated X-ray beam comprising a continuum spectrum of X-rays to a predetermined coordinate and a photon-counting X-ray imaging spectrometer disposed to receive X-rays output from the sample disposed at the predetermined coordinate upon exposure of the sample to the collimated X-ray beam. The X-ray source and the photon-counting X-ray imaging spectrometer are arranged in a reflection geometry relative to the predetermined coordinate.

According to another aspect of the invention, a method for performing X-ray diffraction and X-ray fluorescence on an unprepared sample includes the act of providing an X-ray diffraction and X-ray fluorescence instrument, comprising a broad-spectrum X-ray source and a photon-counting X-ray imaging spectrometer arranged in either a reflection geometry or a transmissive geometry relative to a predetermined coordinate position. The method also includes the acts of placing an unprepared sample at the predetermined coordinate position, outputting a collimated X-ray beam comprising a continuum spectrum of X-rays to the sample, and receiving, at the photon-counting X-ray imaging spectrometer, X-rays output from the sample upon exposure of the sample to the collimated X-ray beam. The method further includes outputting to a processor data corresponding to each X-ray photon registered by the photon-counting X-ray imaging spectrometer, preparing an event list, and analyzing, using the event list, a crystalline texture, crystalline topography, grain size, particle size, and/or time dependence of crystalline structure of the unprepared sample.

According to another aspect of the invention, a method for performing X-ray diffraction and X-ray fluorescence on a sample, whether prepared or unprepared, includes the act of providing an X-ray diffraction and X-ray fluorescence instrument, comprising a broad-spectrum X-ray source and a photon-counting X-ray imaging spectrometer arranged in either a reflection geometry or a transmissive geometry relative to a predetermined coordinate position. The method also includes the acts of placing a sample at the predetermined coordinate position, outputting a collimated X-ray beam comprising a continuum spectrum of X-rays to the sample, and receiving, at the photon-counting X-ray imaging spectrometer, X-rays output from the sample upon exposure of the sample to the collimated X-ray beam. The method further includes outputting to a processor data corresponding to each X-ray photon registered by the photon-counting X-ray imaging spectrom-

eter, preparing an event list, and analyzing, using the event list, a crystalline texture, crystalline topography, grain size, particle size, and/or time dependence of crystalline structure of the sample.

According to still another aspect of the invention, an X-ray diffraction and X-ray fluorescence instrument for analyzing a prepared or an unprepared sample, comprises a X-ray source configured to output a collimated X-ray beam comprising a continuum spectrum of X-rays to a predetermined coordinate and a photon-counting X-ray imaging spectrometer. The photon-counting X-ray imaging spectrometer is disposed to receive X-ray photons output from the sample disposed at the predetermined coordinate upon exposure of the sample to the collimated X-ray beam. The X-ray source and the photon-counting X-ray imaging spectrometer being arranged in either a reflection geometry or a transmission geometry relative to the predetermined coordinate. This instrument also includes a processor and a computer-readable medium bearing instructions configured to cause the processor to carry out the steps of preparing an event list from information output to the processor by the photon-counting X-ray imaging spectrometer and analyzing, using the event list, a crystalline texture, crystalline topography, grain size, particle size, and/or time dependence of crystalline structure of the unprepared sample.

Additional aspects of the invention will be apparent to those of ordinary skill in the art in view of the detailed description of various embodiments, which is made with reference to the drawings, a brief description of which is provided below.

BRIEF DESCRIPTION OF THE DRAWINGS

The file of this patent contains at least one drawing executed in color. Copies of this patent with color drawing(s) will be provided by the Patent and Trademark Office upon request and payment of the necessary fee.

Objects and advantages of the invention will become apparent upon reading the following detailed description in conjunction with the drawings.

FIG. **1** is a schematic representation of a prior art X-ray diffraction apparatus.

FIGS. **2***a*-**2***e* show representations of aspects of embodiments of XRD/XRF devices in accord with aspects of the present concepts.

FIG. **3** shows a representation of aspects of another embodiment of an XRD/XRF instrument in accord with at least some aspects of the present concepts.

FIG. **4** shows a representation of one implementation of an XRD/XRF instrument in accord with at least some aspects of the present concepts.

FIGS. **5***a*-**5***b* depict embodiments of XRD/XRF instruments in accord with still additional aspects of the present concepts.

FIG. **6** depicts a relation between a sample and an origin of a CCD and an X-ray source vector in accord with at least some aspects of the present concepts.

FIGS. **7***a*-**7***e* show results from an analysis of a bulk sample of aluminum-6061 obtained using a prototype XRD/XRF instrument in accord with at least some aspects of the present concepts.

FIG. **8** shows data from a bulk sample of hematite obtained using a prototype XRD/XRF instrument in accord with at least some aspects of the present concepts.

FIGS. **9***a*-**9***c* show data from an aerosol sample obtained using a prototype XRD/XRF instrument in accord with at least some aspects of the present concepts.

FIGS. **10***a*-**10***c* show data from a volatile sample obtained using a prototype XRD/XRF instrument in accord with at least some aspects of the present concepts.

FIGS. **11***a*-**11***b* show data from an organic crystal obtained using a prototype XRD/XRF instrument in accord with at least some aspects of the present concepts.

FIGS. **12***a*-**12***b* represent data that could be expected to be obtained from a powdered sample using a conventional single-wavelength XRD/XRF instrument.

FIGS. **13***a*-**13***b* represent data that could be expected to be obtained from a powdered sample using a multi-wavelength XRD/XRF instrument in accord with at least some aspects of the present concepts.

FIGS. **14***a*-**14***b* represent data that could be expected to be obtained from an unprepared sample using a conventional single-wavelength XRD/XRF instrument.

FIGS. **15***a*-**15***b* represent data that could be expected to be obtained from an unprepared sample using a multi-wavelength XRD/XRF instrument in accord with at least some aspects of the present concepts.

FIG. **16** depicts a comparison between an expected d-spacing measurement resolution and range of the XRD/XRF instrument of FIG. **2***c* to the XRD/XRF instrument of FIG. **1**.

FIGS. **17***a*-**17***b* depict a dual geometry XRD/XRF instrument in accord with at least some aspects of the present concepts.

FIG. **18** shows acts in a method in accord with at least some aspects of the present concepts.

While the invention is susceptible to various modifications and alternative forms, specific embodiments have been shown by way of example in the drawings and will be described in detail herein. It should be understood, however, that the invention is not intended to be limited to the particular forms disclosed. Rather, the invention is to cover all modifications, equivalents, and alternatives falling within the spirit and scope of the invention as defined by the appended claims.

DETAILED DESCRIPTION

While this invention is susceptible of embodiment in many different forms, there is shown in the drawings and will herein be described in detail preferred embodiments of the invention with the understanding that the present disclosure is to be considered as an exemplification of the principles of the invention and is not intended to limit the broad aspect of the invention to the embodiments illustrated. The simplicity, size, weight, configuration, and performance of the apparatus disclosed herein facilitates optimization for and utilization in numerous applications including, but not limited to, manufacturing, scientific, mineralogy, gemological, food industry, pharmacology (e.g., pharmaceutical research, protein folding studies, etc.), medicine, life science, agriculture, agricultural science, law enforcement, defense, security, space, aerosols, and petrochemical applications (e.g., well logging). For example, it is envisaged that a XRD/XRF apparatus **100** in accord with aspects of the present concepts could be utilized as a flight-instrument on a mission to another planet, a planetary or celestial body, or an aircraft. In still other aspects, the XRD/XRF apparatus **100** may be implemented as a portable or even hand-held scanning device that may be used by researchers, police, soldiers, government personnel, engineers, mechanics, or other persons to gather data on objects, materials, or gases of interest. Thus, the presently disclosed XRD/XRF apparatus **100**, as well as methods and techniques disclosed herein, may find application in numerous endeavors and are not limited to any of the disclosed examples.

Referring to FIGS. **2**a-**2**e, the XRD/XRF apparatus **100** is shown to generally comprise a collimated, broad spectrum X-ray source **110** and a charge coupled device (CCD) **120** configured for X-ray detection arranged on opposite sides of a known sample position **125** (i.e., x_0, y_0, z_0), described below. The CCD **120** is positioned to receive X-ray photons **115**, or other energy spectra, output (e.g., diffracted from, fluoresced from, etc.) from the sample **126**.

As shown in FIGS. **2**a-**2**e, a sample **126** to be studied is positioned so that a collimated X-ray beam **105** emitted from the X-ray source **110** strikes the sample at a known position **125** (x_o,y_o,z_o) relative to the CCD(s) **120**. The collimated X-ray beam **105** is, in the depicted geometry of FIGS. **2**a-**2**e, in a plane generally bisecting the CCD **120** through the Y-axis and is parallel to the X-Z plane. However, the X-ray beam **105** need not bisect the CCD **120** through the Y-axis or be parallel to the X-Z plane to obtain useful data in accord with the present concepts. The known position **125** (x_o,y_o,z_o) is selected such that the CCD **120** captures a relatively large solid angle of rays emanating from the sample so that any arbitrary atomic plane separation (d-spacing) can be determined. As shown in the example of FIGS. **2**a-**2**b, for example, the known position **125** (x_o,y_o,z_o) is located near one edge of the CCD(s) **120**.

Although it is certainly preferred to provide a housing or enclosure **101**, such as is shown in FIGS. **2**b-**2**e, a housing is not required for all potential embodiments. The X-ray source **110** is fixed relative to the housing **101** and may be entirely disposed within the housing, partially within the housing, or external to the housing (e.g., with the emitted X-ray beam **105** passed through a window to an interior of the housing). It is preferred that the housing **101** is sealed (or sealable) to maintain a vacuum and correspondingly minimize any potential interactions between the X-ray beam **105** and a gas or gases therein. In some aspects, it may be desirable to include at least a minimal environment of certain gases, such as Helium. In still other embodiments, such as embodiments using higher energy X-ray sources or embodiments used in extraterrestrial applications, the housing environment may be open to the atmosphere or may maintain atmospheres not amenable to lower energy X-ray sources. The housing **101** is optionally shielded.

As shown in the examples of FIGS. **2**a-**2**e, the housing **101** may optionally define a sample aperture **140** adjacent the known position **125** (x_o,y_o,z_o). The size and shape of the sample aperture **140**, also represented in FIG. **2**a, may be freely varied to accommodate the housing **101** configuration and to comport with an anticipated range of uses, desired data, and/or samples, such as shown by way of example in FIGS. **2**c-**2**e. In various aspects of the present concepts, the sample aperture **140** comprises one (or more) fixed window(s) **145** and the known position **125** (x_o,y_o,z_o) is a position flush with, substantially flush with, or adjacent, an underside of the window(s) **145**. The window(s) **145** may comprise any material, or combination of materials (e.g., layers), that is at least substantially X-ray transmissive along the Bremsstrahlung continuum (or a desired subset thereof). For example, the window(s) **145** may comprise a thin beryllium foil or disc, diamond, a polymer (e.g., Mylar™), boron nitride, or silicon nitride. In the example of a beryllium foil or disc, one current embodiment of window **145** is about 75 microns thick (about 0.003"). However, the thickness of the window and window material(s) for a given application vary in accord with variables known to those skilled in the art of X-ray diffraction and fluorescence to, for example, permit transmission of desired energies of X-rays without absorption.

Protective coatings and/or substrates (e.g., BR-127, aluminum, parylene N, DuraCoat™ by Moxtek, BerylCoat-D, gold, electroless nickel, etc.) may also advantageously be applied to the window(s) **145** in accord with anticipated environmental (e.g., temperature) and design considerations (e.g., X-ray energy level) for a given application.

In various aspects of the present concepts, such as are represented in FIGS. **2**a-**2**e, for example, the housing **101** is sealed to form a vacuum environment therein or is selectively sealable to, in combination with a vacuum system, define a vacuum environment therein. In such aspects, the window (s) **145** serve(s) to separate the vacuum volume from the exterior environment to thereby maintain the vacuum environment while permitting X-rays to pass therethrough. However, in another aspect of the present concepts, the window(s) **145** may be omitted so that the sample aperture **140** provides an opening to the outside environment. In still another aspect, the window **145**(s) may be configured as a movable shutter, manually or by a driving device, to selectively occlude the sample aperture during periods of use or non-use.

In other aspects of the present concepts, the optional sample aperture **140** may be omitted and, in lieu thereof, a sample load-lock door (not shown) provided in the housing **101** to permit samples to be introduced into and removed from the housing. In this configuration, the losses due to the use of an X-ray window **145** may be avoided. In aspects thereof, the housing may be evacuated, such as by using a vacuum pump to provide a vacuum of a desired quality.

The X-ray source **110** is optimized to produce a broad spectrum of X-ray wavelengths, such as by producing Bremsstrahlung continuum X-rays spanning between about the 0.1 keV to about the 10 keV band. In at least some aspects, the X-ray source **110** utilizes a 10 keV accelerating field with a high Z element electron impact source, such as gold, to produce Bremsstrahlung radiation with a few characteristic emission lines. In accord with other aspects of the present concepts, different targets and/or different accelerating potentials can be used to further optimize the spectral properties. In still other aspects, plural X-ray sources having the same or different characteristics may be disposed at different positions relative to the known sample position **125** (i.e., x_0, y_0, z_0). The X-rays are then collimated through a pinhole or optical system (e.g., a lens) to produce a small illuminated spot, typically about 1 mm in diameter, on the sample. For small samples, or where a precise location on the sample is to be examined, the sample may be mounted on an XYZ translation stage for positioning in at least some embodiments. Finally, because electron-impact X-ray sources **110** produce optical light, to which X-ray CCDs are sensitive, optical blocking filters, such as aluminized mylar, or baffling may be optionally used to prevent stray optical light from registering on the X-ray CCD **120**.

FIGS. **2**a-**2**e show various embodiments of the sample aperture **140**. FIG. **2**a-**2**b show a sample aperture comprising a circular opening in which a window **145** is fixed. FIGS. **2**c-**2**e show examples wherein the sample aperture **140** comprises a recessed portion in the housing **101**, the recessed portion including a first window **145**a and a second window **145**b in peripheral portions thereof. The recessed sample aperture **140** geometry advantageously minimizes diffraction and fluorescence features from the Be window, achieving an effect similar to the shade **157** in FIG. **2**b. The recessed sample aperture **140** geometry further increases design flexibility by increasing the available options for a fixed input angle for the X-ray beam **105** and a fixed output angle, or range of angles, for diffracted and fluoresced X-rays from the sample **126**. Additionally, by providing two separate win-

dows **145***a*, **145***b*, as opposed to a single window (e.g., **145** in FIG. **2***b*) the surface area of each of the individual window **145***a*, **145***b* is minimized relative to a single window configuration. This permits each of the windows **145***a*, **145***b* to be comparatively thinner than the single window **145**, while retaining the same level of strength against the vacuum drawn in the housing in certain embodiments. FIG. **2***d* shows another variant of FIG. **2***c* comprising an optical lens **146** integrated into a bottom portion of sample aperture **140** (i.e., the "top" of the recessed portion, as shown). FIG. **2***e* shows a variant of FIG. **2***d* wherein a shutter is provided over the optical lens **146**. The sample aperture **140** is not limited to the depicted configurations and may assume any configuration sufficient to permit X-rays (or other spectra of energy, such as optical light) from the X-ray source **110** to leave the housing **101** and to permit X-rays (or other spectra of energy) **115** output from a tested sample to enter the housing for registration on one or more appropriately configured energy detectors.

In the aspects shown in FIGS. **2***b*-**2***e*, a collimator **155** is provided in the form of a brass tube having a proximal end disposed on or adjacent the X-ray source **110** and distal end disposed adjacent the window **145**. A pinhole **156** is formed at the distal end of the collimator **155**. Alternatively, other forms of collimator (e.g., lens(es), plates, shutters, etc.) may be used. In the embodiment of FIG. **2***b*, a shade **157** is also provided at the distal end of the collimator **155** to block X-rays diffracting and fluorescing from the window **145**. In the embodiments of FIGS. **2***c*-**2***e*, the distal end of the collimator **155** is disposed to abut, or at least substantially adjacent to, a first window **145***a* that is inclined relative to a bottom of the housing **101**. In these aspects of FIGS. **2***c*-**2***e*, a second window **145***b* is similarly inclined relative to a bottom of the housing **101**. The second window **145***b* is configured to transmit the diffracted and fluoresced X-rays from the sample toward the CCD **120**. As shown in FIGS. **2***c*-**2***e*, the CCD **120** may be advantageously tilted toward the second window **145***b* by any desired angle θ_C (e.g., between about 0-45°, or greater angles, if desired). Likewise, the angle at which the first window **145***a* and second window **145***b* may be tilted may also assume any desired angle.

In FIG. **2***d*, the housing **101** is divided into a first vacuum chamber **102** and a second vacuum chamber **103** by a wall **106**. An optical CCD **121** is disposed within the housing **101** in the first vacuum chamber **102** above the sample aperture **140** such that optical light transmitted through the optical (focusing) lens **146** from the sample **126** is incident upon the optical CCD. The wall **106** (i.e., a light-tight partition) serves to prevent stray optical light from introducing background noise on the X-ray CCD **120** and does not interfere with the diffracted and fluoresced X-rays leaving the sample **126** and going toward X-ray CCD **120**. Thus, in the example of FIG. **2***d*, the XRD/XRF apparatus **100** provides for both X-ray imaging and optical imaging, simultaneously or separately.

FIG. **2***e* shows another variant wherein the wall **106** of FIG. **2***d* is omitted in favor of a mirrored surface **107** positioned to intercept and reflect incident optical light transmitted through optical lens **146** toward the X-ray CCD **120**. In this configuration, the X-ray CCD **120** is utilized to perform optical imaging of the sample **126**. A movable or actuatable shutter **147** is provided between the optical lens **146** and mirrored surface **107** and preferably adjacent the optical lens so as to selectively cover or expose the optical lens. The X-ray data and optical data could not be acquired at the same time in this configuration and the shutter **147** would be used to control optical exposures. In at least some aspects, the powering of the X-ray source **110** on and off could be used to control X-ray data acquisition.

The embodiments shown in FIGS. **2***d*-**2***e* recognize that, in many applications, there is significant value in being able to examine visually a sample that is undergoing XRD and XRF analysis. For example, mineral identification is simplified considerably when optical characteristics such as color, reflectivity, and surface texture are available. Another advantage of optical imaging is that it allows for precise and reproducible positioning of samples. An illumination source, not shown in FIGS. **2***d*-**2***e*, may be optionally provided to enhance optical imaging. In at least some aspects, the illumination source may comprise one or more white LEDs disposed adjacent the sample aperture **140** and/or adjacent the optical lens **146** to illuminate a sample. In another aspect, an illumination ring or rings (e.g., white light) may circumscribe a periphery of the optical lens and/or the sample aperture **140**. Further or alternatively, one or more light sources having different characteristics (e.g., ultraviolet light (UV-A, UV-B, UV-C), infrared, etc.) may be utilized to provide enhanced analysis capabilities (e.g., fluorescence, phosphorescence, optically stimulated luminescence, triboluminescence, etc.).

The CCD **120** is coupled to CCD control and readout electronics **130**, which in turn communicates, via a suitable hardwired or wireless communication path and/or communication interface, with a processor **135** configured to execute one or more instruction sets relating to event processing. From the X-ray capture event data output by the CCD **120**, the processor **135** is able to generate a four-dimensional event list from the measured time, X-position, Y-position, and energy of each X-ray, data which will be described in greater detail below.

The CCD **120** comprises an array of pixels optimized for X-ray detection. In such a configuration, the CCD **120** can detect individual X-ray photons **115** and output to the processor **135**, through the CCD control and readout electronics **130**, information on the X-position and Y-position where the photons strike the CCD, as well as the energy (and thus the wavelength) of the individual X-ray photons. The CCD **120** continuously reads out images that are processed to extract the individual X-ray events containing position and energy information for each photon detected. As the CCD **120** information is received by the processor **135**, individual photon events are identified and the event processing instruction sets, hardware, and/or firmware compiles a list or database of individual X-ray events. Each X-ray event is associated with a time (e.g., with resolution of the readout rate, typically seconds), position (e.g., X-position, Y-position), and energy (E). The processor **135** is operatively associated with at least one memory device (not shown) bearing the instruction set(s) controlling the event processing data operations and/or analyses and output devices for conveying information to a user. Execution of the sequences of instructions contained in the memory causes the processor **135** to perform the process steps described herein. Although the processor **135** is described in a singular form, the processor may comprise one or more processors in a multi-processing arrangement. The memory may comprise any computer-readable medium configured to store data and permit access thereto by a processor for execution including but not limited to, non-volatile media (e.g., optical or magnetic disks), volatile media (e.g., dynamic memory), and transmission media (e.g., signals received over coaxial cables, copper wire, fiber optics, or carrier waves, such as acoustic or light waves generated during radio frequency (RF) and infrared (IR) data communications). The processor **135** is also advantageously associated with a communication interface (e.g., ISDN card, modem, etc.) configured to provide data communication capability (e.g., transmission only or two-way coupling) to an external processor,

computer, or network. In any such implementation, the communication interface would send and/or receive electrical, electromagnetic or optical signals that carry digital data streams representing various types of information.

In at least some aspects of the present concepts, the CCD **120** is a square or rectangular array having a width and height of several centimeters (e.g., 2.0, 2.5, 3.0, 3.25, 3.50, 3.75, 4.00, any values therebetween, etc.) with a pixel size of about 20-25 microns, or smaller. However, in still other aspects, the CCD **120** may comprise a larger CCD than the noted example (e.g., greater than 4.00 cm), a plurality of tiled or adjacently-disposed CCDs, and/or one or more non-planar CCDs. Thus, a plurality of CCDs **120** may be used to increase the area over which spectroscopic images are available, such as by disposing a plurality of CCDs (or other type of X-ray detector) around the known sample position **125** (i.e., x_0, y_0, z_0) and/or sample aperture **140**, if provided, such as is shown by way of example in FIG. **3**.

FIG. **3** shows a mosaic of CCDs **120** positioned to at least partially circumscribe the known sample position **125** (i.e., x_0, y_0, z_0) and sample aperture **140** to provide wide solid angle coverage. For example, the mosaic of CCDs **120** may span an arc of between about 180° up to and including 360°, or may span a lesser arc (e.g., 15°, 30°, 45°, 60°, 90°, 120°, or any smaller angle or intermediary angle, etc.). As shown in the example depicted in FIG. **3**, the mosaic of CCDs **120** may span an arc slightly greater than about 180°. In still additional configurations, a plurality of CCDs **120** may be disposed to further provide X-ray detection capability along an upper portion of the XRD/XRF apparatus **100** (e.g., over known sample position **125** (i.e., x_0, y_0, z_0)). Such arrangements of CCDs may assume any geometry or shape, including for example, a hemispherical shape, a spherical frustum, or a polyhedral shape. Such multi-CCD **120** configurations provide a larger d-spacing range and/or finer d-spacing resolution, and increased sensitivity.

The CCD **120** is, at in some aspects of the present concepts, disposed in a housing **101** serving as a vacuum chamber. The CCD **120** is cooled to, for example, reduce thermally generated electrons in the detector and increase signal to noise ratio. However, cooling of the CCD **120** is not mandatory in all embodiments and it is expected that room temperature X-ray CCDs will be available in the near future.

The energy resolving power of the CCD **120** is energy dependent (e.g., the energy resolving power of the CCD **120** is typically about 2% at about 6 keV). The energy dependence of the energy resolution (full width at half-maximum, in eV) is given by:

$$\Delta E_{FWHM}=2.354\times 3.65\times (N^2+FE/3.65)^{1/2} \quad (1)$$

where N is the readnoise in electrons of the CCD and typically is 5 electrons, F is the "Fano Factor" for silicon and is typically about 0.1, and E is the photon energy in eV. X-ray CCDs differ from the usual CCD in that their detection volume (the "depletion" region) is thicker so as to make it more sensitive to more penetrating radiation. To achieve the deep depletion the base material of the X-ray CCD is of a higher purity and thus higher-resistivity silicon than in normal optical CCDs. As discussed below (see, e.g., FIG. **16**), the single-photon energy measurement capability of the CCD **120**, or other X-ray detector, is the dominant term in the "error budget" that determines the d-spacing measurement resolution of a continuum spectrum of X-rays based diffraction instrument.

Referring back to FIGS. **2***a*-**2***b*, for example, X-rays coming from the sample produced by fluorescence (XRF) are emitted with no specific directionality and will be captured by the CCD **120** with no spatial patterning, apart from $1/r^2$ and solid angle projection effects. The XRF X-rays, however, carry information about the elemental make-up of the sample through the characteristic X-ray lines they emit. In this regard, it is noted that the reflection geometry provided by the XRD/XRF apparatus **100** provides less self absorption in the sample than is possible in a transmission geometry, allowing for the measurement of lower energies and for the performing of a better and more quantitative calibration procedure. Still further, for a given d-spacing range and resolution, the XRD/XRF apparatus **100** can use a X-ray beam **105** having comparatively larger spot sizes (e.g., about 1 mm in diameter rather than about 0.05 mm in diameter) to provide a larger XRF signal for the same X-ray source **110** power. Use of a continuum spectrum of X-rays to excite XRF in the sample up to the cutoff energy of the X-ray source **110**, as opposed to using a characteristic line to excite XRF in the sample up to a much lower energy, allows the XRD/XRF apparatus **100** to more efficiently and completely excite XRF than conventional XRD/XRF apparatus **10** and techniques. For example, for conventional XRD/XRF apparatus **10** using Co Kα X-rays from the source, which is less efficient at exciting XRF from, for example, Sulfur than continuum photons (as utilized in the XRD/XRF apparatus **100** disclosed herein) just above the S-K edge while such Co Kα X-rays are incapable of exciting XRF from higher Z elements, such as Fe or Ni.

Diffracted X-rays, in contrast, emerge from the sample in specific directions consistent with Bragg's law:

$$n\lambda=2d\,\mathrm{SIN}(\theta) \quad (2)$$

where λ is the wavelength of the X-ray photon, d is the atomic plane spacing for the tested material, 2θ is the diffracted angle, and n is the diffraction order. The diffraction angle θ is coded in the X-Y plane of the CCD **120**. In FIG. **2***a*, the dashed arc **122** in the CCD **120** X-Y plane represents, for example, where a diffracted angle of 2θ would intersect the CCD. Generally, as the CCD **120** X-position increases, so does the diffraction angle.

When the collimated X-ray beam **105** strikes the sample, some of the X-rays forming the X-ray beam are diffracted in accordance with Bragg's Law. The strongest X-ray diffraction occurs when the angle of X-ray incidence on an individual series of atomic planes equals the angle of exit (i.e., specular reflection). Some of the X-rays are stopped in the sample where the energy deposited thereby causes individual atoms to produce characteristic X-ray emission lines with known wavelengths through X-ray fluorescence (XRF). Whereas monochromatic X-rays striking a sample containing crystallites of a given atomic-plane spacing d and oriented in slightly different directions may result in constructive interference from just one of the crystallites, as determined by Bragg's law, providing a range of wavelengths in accord with the present concepts permits accommodation of a range of crystallite orientations and extends the instrument's ability to probe the crystal structure of the sample. The CCD **120** captures a large solid angle of both diffracted and fluoresced X-rays and outputs the event information to the processor, as noted above, where the processor assimilates the event information and produces an event list describing the interaction points (x, y, z), wavelength (λ), time and/or energy (E) of each individual X-ray photon detected by the CCD **120**. The event list may comprise any subset of the aforementioned data (e.g., only x-position, wavelength, and energy, etc.) and is not required to include all of the above data points.

The event list data can be filtered to examine particular subsets of information including, for example, plotting only

those photons consistent with diffraction from a single d-spacing to thereby directly image the size and orientation distributions for crystal grains containing that d-spacing. Furthermore, because photon detections are optionally time-tagged (with the intrinsic resolution of the X-ray detector), time-dependent material analysis is also possible in accord with at least some aspects of the present concepts. Time-tagging, together with the high sensitivity of the XRD/XRF instrument **100**, allows for measurements of phenomena that evolve with time such as, but not limited to, changing crystal structure (e.g., d-spacings, degree or quality of crystallization in growth and degradation, grain sizes and shapes, crystal texture, etc.) or changing chemical makeup (e.g., monitoring elemental abundances through XRF during a chemical reaction, etc.). Further, as to crystal texture analysis, the methods described herein fully exploit the XRD/XRF instrument **100** data to compute d-spacings for individual photons, filtering event lists for successive d-spacing values and plotting the resulting detector images, optionally in polar coordinates to eliminate distortion. Photons are presently tagged with a readout time with a resolution of a few-seconds resolution. However, faster CCD **120** readout electronics and/or utilization of a pulsed or modulated X-ray source **110** can improve this time resolution.

FIG. **4** shows one embodiment of at least some aspects of a XRD/XRF instrument **100** in accord with the present concepts. The XRD/XRF instrument **100**, comprising the broad spectrum collimated X-ray source **110** and the CCD **120** are disposed in a small sensor head **400**. The sensor head **400** is connected to a control system **485** via a cable **415**. The local control system **485** comprises, for example, CCD control and readout electronics, processor(s), memory, power supply, and associated software, firmware, and/or hardware necessary to perform event processing for the CCD **120** event data.

The sensor head **400** may be made to be less than about 5 centimeters on a side and is mountable, if desired, on a robotic arm (not shown), such as may be provided on an extraterrestrial landing vehicle, law enforcement robotic vehicle, or the like. The sensor head **400** may optionally comprise shielding to eliminate any X-rays not originating from X-ray source **110**. In operation, the sensor head **400** would be placed on top of a sample so that a portion of the sample disposed at the known sampling position **125** (x_o, y_o, z_o) could be illuminated by the X-ray beam (not shown). One or more sensors such as, but not limited to, a touch sensor, laser range finder, or mechanical rest may be advantageously utilized to ensure the sample is appropriately positioned. The data would then be output via a cable **415**, or via some other suitable wired or wireless communication path, to an associated processor **135**, whether disposed in the local control system **485** or remotely disposed.

In at least some aspects, the software, firmware, and/or hardware (e.g., electronics) required to control the operation of the sensor head **400** (e.g., CCD controller, event extractor, computer interface, event logger, and/or other software, firmware, and/or hardware) may be integrated within or on the sensor head and/or may be disposed remotely, in whole or in part, in the robotic vehicle or other platform external to the sensor head. Electrical communication between the sensor head **400** and any remote software, firmware, and/or hardware may be achieved by use of a flexible signal cable (e.g., a cable routed through or on a robotic arm) and/or wireless communication device(s) (e.g., using Bluetooth or other wireless communication protocol). Power may be provided to the sensor head **400** the robotic vehicle or other platform through cable **415** or through a dedicated power cable, preferably routed directly through or on the robotic arm (not shown).

In any portable unit, such as sensor head **400**, the CCD **120** and X-ray source **110** vacuum volumes (e.g., vacuum chamber of housing **101** or separate vacuum chambers) would have to be maintained without large mechanical, cryogenic, or diffusion pumps. In these instances, techniques similar to those used for commercial sealed electronic X-ray tubes (e.g., heat- or chemically-activated gas getters) may be employed. Welded joints and/or metal gaskets may be used in lieu of rubber or viton to minimize permeability of the sensor head **400**. These approaches may facilitate further miniaturization of embodiments of the disclosed XRD/XRF instrument **100** deployed in a sensor head **400**.

It is to be understood that the present concepts are not limited to any particular size, arrangement, or geometry of CCD(s) **120**, subject to the above-noted requirement to sufficiently resolve the position and energy of individual X-ray photons and output to a processor information relating thereto. In at least one embodiment, the CCD **120** may comprise the Event Driven CCD (EDCCD), Gen 1.0 device, or successor devices, fabricated at the Massachusetts Institute of Technology (MIT) Lincoln Laboratory. The apparatus and methods disclosed herein are not limited to a CCD **120** X-ray detector or detectors and, in various aspects, may utilize a X-ray detector other than a CCD **120**, such as another type of solid-state imaging X-ray detector (e.g., active pixel silicon detectors), single-photon spectroscopic area detector, combinations of CCDs with other detectors (e.g., CCD to cover low energy part of XRD/XRF work with CZT array to cover diffraction or scattering of higher energy X-rays or large, cheap imaging proportional counters in combination with strategically located CCDs), Tunnel Junction detector arrays, X-ray microcalorimeter arrays, and/or imaging proportional counter. As noted above, the energy resolution of the selected energy-resolving imaging photon-counting detector will drive the performance of the XRD/XRF instrument **100** in regards to d-spacing resolution (see, e.g., FIG. **16**).

FIG. **5***a* shows one embodiment of at least some aspects of the present concepts wherein the XRD/XRF instrument **100** is configured to provide real-time aerosol collection and analysis. As with the previous examples, the X-ray source **110** is configured in a reflection geometry to output an X-ray beam **105** to a known position (x_0, y_0, z_0) (not shown) from which point X-rays **115** are diffracted toward CCD **120**. However, it is to be noted that these concepts are not limited to real-time aerosol collection and analysis in a reflection geometry and the concepts described herein apply equally to aerosol analysis of a prepared or unprepared sample in transmission geometry (e.g., using a thin collecting tape, using a disk system and rotating the disk like a filter wheel with discrete positions or even continuously in front of the X-ray beam, etc.). In the depicted example of FIG. **5***a*, particles are collected on a tape **148** aerosol collection substrate **150** by impactation, filtration, or electrostatic precipitation (e.g., needle to plate electrostatic precipitator), and then the substrate **150** is moved (e.g., automatically) by a drive system to the sample aperture **140** for analysis. The tape **148** may comprise, but is not limited to, a polycarbonate or other synthetic material. In at least some aspects, the collecting tape may comprise a first roll **155** of tape bearing a supply of clean aerosol collection substrate and a second, take-up roll **156**. In another alternative embodiment, the reels **155**, **156** may be omitted and an aerosol collection substrate holder, port, or ported vacuum chamber may be provided to hold an aerosol collection substrate **150** (e.g., manually or automatically inserted) during analy-

sis. Optical probes (not shown) may optionally be provided externally to the XRD/XRF instrument **100** to provide complementary information on size, refractive indices, etc.

FIG. **5***b* shows yet another embodiment of at least some aspects of the present concepts wherein the XRD/XRF instrument **100** is configured to provide a real-time "flyby" particle measurement system. As with FIG. **5***a*, the X-ray source **110** is configured in a reflection geometry to output an X-ray beam **105** to a known position (x_0, y_0, z_0) (not shown) from which point X-rays are diffracted toward CCD **120**. In this example, particles **160** are not collected on an aerosol collection substrate, but are rather measured while suspended in the atmosphere. Particles may include, for example, but are not limited to, aerosols or ice.

FIG. **6** shows an illuminated spot of a sample material and highlights the deriving of the quantity 2θ for an arbitrary position on the CCD **120**.

A coordinate system is established with an origin at a pixel (row 0, column 0) of the CCD **120**, with the CCD shown to lie in the (x,y) plane. Unit vectors are shown. The incoming photon direction is defined by the vector $\hat{p}$ (i.e., the X-ray source vector) and the diffracted beam is defined by the vector $\hat{q}$, with the illuminated spot on the sample at position (x_0,y_0,z_0). For the following illustrative remarks, it is assumed that $\hat{p}$ lies in the (x,z) plane.

The incoming and outgoing photon vectors may be defined as follows:

$$\hat{p} = -\sin\theta_\gamma \hat{x} - \cos\theta_\gamma \hat{z} \tag{3}$$

$$\hat{q} = \frac{\vec{q}}{|\vec{q}|} = \frac{(x-x_0)\hat{x} + (y-y_0)\hat{y} - z_0\hat{z}}{\sqrt{(x-x_0)^2 + (y-y_0)^2 + z_0^2}}. \tag{4}$$

Then:

$$\cos(2\theta) = \hat{p}\cdot\hat{q} = \frac{-\sin\theta_\gamma(x-x_0) + \cos\theta_\gamma z_0}{\sqrt{(x-x_0)^2 + (y-y_0)^2 + z_0^2}}. \tag{5}$$

Bragg's law links d to sin(θ), so the following trigonometric identity is useful:

$$\cos(2\theta) = 1 - \sin^2\theta. \tag{6}$$

It is possible, then, to compute d as a function of photon position and energy, without any trigonometric computations:

$$d = \frac{n\lambda}{\sqrt{2 - 2\cos(2\theta)}}, \tag{7}$$

where cos(2θ) is given above (note that $\sin\theta_\gamma$ and $\cos\theta_\gamma$ are constants for a fixed geometry). To derive azimuthal angle, ϕ, around a diffraction cone intercepted by a flat surface, the origin is first translated (in all three dimensions) to the illuminated spot on the sample, so that an arbitrary point (x_d, y_d) on the detector has coordinates

$$(x,y,z) = (x_d - x_0, y_d - y_0, -z_0) \tag{8}$$

The coordinate system is then rotated by $-\theta_\gamma$ (i.e., clockwise) about $\hat{y}$, so that the z' axis is anti-parallel to the incoming photon direction. The pixel coordinates under this rotation transform to:

$$x' = x\cos\theta_\gamma - z\sin\theta_\gamma$$

$$y' = y$$

$$z' = x\sin\theta_\gamma + z\cos\theta_\gamma. \tag{9}$$

Because the vertical axis is now aligned with the axis of the diffraction cone, the azimuthal angle around the cone is just

$$\begin{aligned}\phi &= \tan^{-1}\left(\frac{y'}{x'}\right) \\ &= \tan^{-1}\left[\frac{y_d - y_0}{(x_d - x_0)\cos\theta_\gamma + z_0\sin\theta_\gamma}\right]\end{aligned} \tag{10}$$

The intersection of a cone and a plane traces out a circle, ellipse, parabola, or hyperbola depending on the relative orientations of the cone's symmetry axis, its "generator" lines, and the plane's normal vector. The only case in which diffraction arcs on a CCD will be circular is in the transmission configuration where $\theta_\gamma=0$. In reflective geometries, such as relates to the disclosed examples of FIGS. **2***a*-**2***e*, **3**, **4**, and **5***a-b*, for $\theta_\gamma>0$, the diffracted X-rays form arcs on the CCD **120**, or other detector, that are parts of ellipses, a parabola, and hyperbolae, all at the same time, depending on the value of θ_γ relative to 2θ. The arc will be part of an ellipse if $2\theta<(\pi-\theta_\gamma)$, part of a parabola if $2\theta=(\pi-\theta_\gamma)$, and a hyperbola if $2\theta>(\pi-\theta_\gamma)$.

The derivations above assume that CCD positions (x,y) are known and the polar angles (θ,ϕ) must be solved for, as is appropriate for analyzing data. In a simulation, however, we will typically want to specify the crystal(lite) orientations (θ,ϕ) and solve for the detector coordinates of diffracted photons. To simulate a powder sample, for example, the azimuthal angle ϕ would be drawn from a uniform distribution, while the mineral d-spacing and photon wavelength determine θthrough Bragg's law.

Using the following definitions, $C\equiv\cos(\theta_\gamma)$, $S\equiv\sin(\theta_\gamma)$, $Z\equiv z_0$, $P\equiv\tan(\phi)$, and $T\equiv\cos(2\theta)$, the equations for cos(2θ) and tan(ϕ) above can be merged and the quadratic solved for $X\equiv x-x_0$ and $Y\equiv y-y_0$:

$$\begin{aligned}X &= \frac{-b + \sqrt{b^2 - 4ac}}{2a} \\ Y &= P[XC + ZS]\end{aligned} \tag{12}$$

wherein the second root for X is only of interest in transmission geometries, and where

$$a = T^2(1+P^2C^2) - S^2$$

$$b = 2SCZ(1+T^2P^2).$$

$$c = Z^2(T^2 + T^2P^2S^2 - C^2) \tag{13}$$

The placement of the sample (e.g., sample **126** in FIG. **2***b*), at the known position **125** (x_o,y_o,z_o) may be advantageously facilitated by one or more sensors (not shown) disposed in or adjacent the known position (x_o,y_o,z_o), sample aperture **140**, and/or window **145**. Such sensor(s) may include, but are not limited to, physical devices (e.g., pressure sensor, force sensor(s), resistive touch screen panel/overlay, surface acoustic wave touch screen panel/overlay, guided wave touch screen panel/overlay, infra-red touch screen panel/overlay, contact switch(es), proximity switch(es), etc.) or optical devices (e.g., laser(s), camera, devices, etc.). To the extent that a

sample may not be precisely positioned at the known position **125** (x_o,y_o,z_o), the positional data output by the sensor(s) may be advantageously utilized by the processor to introduce corrections or transformations, as needed, for the data obtained from CCD **120**.

To compute diffraction angles from detector coordinates, the collimated X-ray beam **105** direction and the position of the illuminated spot on the sample **126**, relative to the detector **120** origin, must be known. Although the X-ray beam **105** direction and location are constant for a given XRD/XRF instrument **100**, the placement of the sample **126** and irregularities in its shape can alter the precise location of the illuminated spot. In practice, incoming rays may be slightly converging or diverging, while the illuminated spot will have some non-zero extent, usually in x and z. These complications can degrade the d-spacing measurement resolution, but their effects are easily modeled and limited. In the simple configuration of FIG. **2***a*, the geometry is fully characterized by three parameters: x_0, z_0, and θ_γ, with y_0 fixed by construction (e.g., along the centerline of the CCD **120** in FIG. **2***c*). The values of these parameters can be derived, if no other means exists to measure them directly (e.g., optical imaging), by obtaining data from a calibrator sample, any substance that exhibits at least three d-spacings within the XRD/XRF instrument's **100** range. Aluminum serves very well (see FIGS. **7***a*-**7***e*) for this purpose. Because two of the three parameters (the slope θ_γ and an intercept) describe the fixed X-ray beam **105** line, they apply equally to all other datasets acquired with the same XRD/XRF instrument **100**, leaving only a single parameter (i.e., position along the beam line) to be solved for subsequent samples. This can be accomplished by, among other means, cumulating d-spacing histograms over a range of possible sample positions and choosing that which produces the highest signal-to-noise ratio peaks.

The CCD **120** accumulates photons for a fixed exposure time (e.g. 10 seconds or less), putting out a sequence of images which are then processed to extract the individual X-ray events containing position and energy information. CCD **120** readout electronics produce an amplified signal proportional to the charge produced in each pixel by ionizing X-ray photons. To perform single-photon spectroscopy, this pixel charge information must be scanned and analyzed for local excesses, possibly distributed over multiple pixels. Techniques to accomplish this have been refined and are well known in the field of X-ray astrophysics. For field units, these algorithms may be implemented on field programmable gate array (FPGA) electronics for portability and speed of execution. As the CCD **120** is read out and individual photon events are identified, a list of single-photon properties is compiled by the processor **135** in an event list comprising time (with resolution of the readout rate), position, and energy.

The CCD **120** is reporting θ and ϕ (the azimuthal angle along diffraction cones) encoded in X and Y, as well as energy for all events. The energy (E) measured by the CCD **120** may be converted into a wavelength λ using the quantum physical relation:

$$\lambda = hc/E \tag{14}$$

where h and c are Planck's constant and the speed of light, respectively, and the product hc=12400 eV-Å. The X-ray source is producing a broad bandpass of λs. By plotting E vs. θ for all the X-ray events in the event list, it can be seen how the diffracted X-rays differentiate themselves from XRF X-rays. Specifically, related XRF information appears as a constant in the E vs. θ space, while related diffracted X-ray photons would follow (reciprocal) SIN functions with amplitude proportional to twice the atomic plane spacing (d) of the material in the sample. Thus the XRD/XRF instrument **100** is simultaneously providing elemental composition from the XRF data as well as more specific atomic plane spacing (d) information from the XRD data. Combined, this information can then be used to identify the sample.

If Bragg's Law (Eq. 2) is applied to the geometry described above, data from each event may be used to convert x and y to diffraction angle θ and cone azimuth ϕ, convert event energy to wavelength λ, and calculate the expected d-spacing if that event was due to XRD. From this information, the data may be plotted in the space of energy vs. d-spacing, where XRF and XRD features of interest are orthogonal (e.g., FIG. **7***b*, discussed below). In these diagrams, the "banana" envelope of the photon events reflects the boundaries of the CCD detector in 2θ, consistent with Bragg's law. For the Al 6061 sample data in FIGS. **7***a*-**7***e*, this envelope corresponds to 38° along the upper boundary, and 72° along the lower boundary. To form crude energy and diffraction spectra, this two-dimensional information can be collapsed horizontally and vertically. For quantitative analysis of a diffraction spectrum ("diffractogram"), however, it is important to account for the different energy bandwidths/bandpasses and detector areas that are cumulated into the various diffractogram bins. This normalization changes the relative ratios of the amplitudes of diffractogram peaks, which carry information about mineral phase, mineral abundances, and crystal texture. Both normalized and unnormalized diffraction spectra are plotted in some of the sample data discussed below. Mixed XRD/XRF data may be analyzed, in accord with at least some aspects of the present concepts, through energy filtering, 2-D Fourier filtering (E vs. 2θ or E vs. d), and/or 2-D simultaneous matched filtering. Diffractograms are normalized per energy bandwidth and detector area.

The XRD/XRF instrument **100** described herein captures additional information as well due to specular reflection (i.e., perfect reflection in which an X-ray from a single incoming direction (θi) relative to a surface normal is reflected into a single outgoing direction (θr) relative to the surface normal wherein θi is equal to θr). If, for example, the sample **126** disposed at the known sample position **125** in FIG. **2***b* were a perfect crystal with atomic planes disposed parallel to the Y-Z plane, then the brightest X-ray diffraction peak would occur at an angle equal to the incident angle of the collimated beam **105** on the sample. This would happen at a particular wavelength (λ) consistent with Bragg's Law (Eq. 2). Since the X-ray source **110** produces a broad range of wavelengths λ, this condition will be satisfied. Further, the CCD **120** X-Y image defines an image of the X-ray source **110** with a size comparable to the footprint of the collimated X-ray beam **105** on the crystal. If the crystal in this example were to be tipped toward the CCD (i.e., rotated about the Y-axis) then the image would move along the X direction of the CCD (and the wavelength would change). If the crystal were rotated about the Z-axis, then the image would shift azimuthally along an arc of constant 2θ. If the crystal were smaller than the footprint of the collimated X-ray beam striking the crystal, then the size and shape of the reflected image would correspond to the crystal's size and shape. If the sample is composed of many small crystal or domain facets, then the image would describe the granularity and crystalline texture of the sample by providing size and orientation (i.e., tip-tilt of crystal grains) distribution information.

The use of Bremsstrahlung continuum X-rays, or a "white light" approach, to XRD and XRF in accord with the present concepts provides many important advantages over traditional monochromatic techniques. At the same time, this

broad spectrum approach presented a data-reduction challenge regarding the simultaneous analysis of XRD and XRF features in the same broadband data stream. In accord with the present concepts, the diffraction and fluorescence properties of a sample can be isolated and characterized with varying levels of sophistication, such as by alternately masking out horizontal or vertical features in energy vs. d diagrams (e.g., FIG. **7***b* or FIG. **8**), by applying a Fourier filter to the image, or by simultaneously fitting all observed features to a model of the instrument and the sought-after properties of the sample. Other forms of analysis, whether conventional analysis tools in X-ray astrophysics or analysis tools yet to be developed are all utilizable in accord with the present concepts. The first approach noted above, masking, is trivial to implement and provides gross separation of the XRF and XRD information. The second approach, two-dimensional Fourier filtering, neatly distinguishes, in most cases, the horizontal and vertical features, allowing for standard fluorescence and diffraction (e.g., Rietveld) analyses on the resulting one-dimensional spectra. The third approach, simultaneous fitting, involves applying an accurate model of the instrument's response to a variety of assumed source properties and fitting for the best match. A high-fidelity model of the instrument allows for well-calibrated datasets, while simultaneous fitting for fluorescence and diffraction increases sensitivity to weak features.

A first and a second prototype XRD/XRF instrument **100** in accord with the present concepts were built and respectively correspond to FIGS. **2***a* and **2***b*. A third prototype XRD/XRF instrument **100** is being built to correspond to the arrangement depicted in FIG. **2***c*. The first and second prototypes comprise(d) a 10 keV electron impact X-ray source (Austin Instruments, Model 2—Mason Source) and a commercially available X-ray CCD **120** with 20 micron pixels (Princeton Instruments Model 7509-0007 and Princeton Instruments Model 7510-0006, respectively). Data samples described below are from the second prototype (see FIG. **2***b*), which comprises a 1340×1340-pixel CCD **120** (26.8 mm×26.8 mm active area). The X-ray source **110** comprises a gold-plated (Au) copper (Cu) target to produce strong Bremsstrahlung continuum, as well as Au M characteristic lines (e.g., $M_{\alpha 1}$, $M_{\alpha 2}$, M_{β}, M_{γ}). Referring to the configuration depicted by way of example in FIGS. **2***a*-**2***b*, the first prototype XRD/XRF instrument **100** was configured with θ_{γ}=28.5° relative to the Y-Z plane and x_o=−1.9 mm, y_o=4.0 mm, and z_o=33 mm relative to the lower right corner of the CCD **120**. The second prototype XRD/XRF instrument **100** was configured with θ_{γ}=30.0 degrees and a known sample position **125** at coordinates of x_o=−3.9 mm, y_o=13.4 mm, and z_o=34.7 mm, all measured relative to the lower right corner of the CCD **120**. The third prototype XRD/XRF instrument **100** was configured with θ_{γ}=30.0 degrees and a known sample position **125** at coordinates of x_o=4 mm, y_o=13.4 mm, and z_o=25 mm, all measured relative to the lower right corner of the CCD **120**. The beam current was variable between 50 and 300 micro-Amps. For the following examples, no sample preparation was performed. The samples were merely disposed at the known sample position **125** (x_o,y_o,z_o). The X-ray spot size on the samples was an ellipse with major and minor axes of 2 mm and 1 mm, respectively.

In the above-noted second prototype XRD/XRF instrument **100**, the time resolution was limited by the readout rate (~2 seconds) of the commercial X-ray CCD **120** and the fact that each frame must be exposed for a period significantly longer (~10 seconds) than the readout rate to reduce contamination of images by "misplaced charge." Misplaced charge is the effect of having photons land physically in the correct part of the device, but during the readout, so that in the final image the registered charge is smeared along the readout direction. The effects of misplaced charge are evident in, for example, the data shown in FIG. **11***b*. The misplaced charge due to readout rate may be improved by using faster CCD devices, or other technologies (e.g. event driven CCD).

In the data samples described below, the CCD **120** is kept in a vacuum chamber (i.e., housing **101** in this example) with the X-ray source **110**. The CCD **120** of the prototypes is chilled, but room temperature X-ray CCDs are expected to become available in the near future and are expected to be utilized in other implementations of the present concepts. For convenience, as shown in FIG. **2***b*, the sample **126** is kept in air and the X-ray window **145** (e.g., a 0.003" thick Beryllium sheet) separates the vacuum volume inside housing **101** from the exterior environment. As noted above, a shade **157** is provided at the distal end of the collimator **155** to block X-rays diffracting and fluorescing from the window **145**. In a third prototype, currently nearing completion and represented generally by FIG. **2***c*, the X-rays diffracted and fluorescing from the X-ray window **145***a* (e.g., Beryllium) are virtually eliminated by providing a second, separate window **145***b* as any X-rays diffracted and fluoresced from the window **145***a* are not incident to the CCD **120**. In the illustrated configuration of FIG. **2***c*, the CCD is disposed at an angle θ_C of about 10° to capture a larger range of diffraction angles. The XRD/XRF instrument **100** represented in FIG. **2***c* provides a geometry allowing work at large d-spacings and is expected to improve the efficiency of the system by allowing the X-rays to pass through windows at nearly normal incidence, which minimizes absorption.

Example 1

AL 6061

FIGS. **7***a*-**7***e* show results from a piece of aluminum-6061 obtained using the second prototype XRD/XRF instrument **100** in a 2-hour data run with the X-ray source **110** operating at an electron beam current of 100 microamps. FIG. **7***a* shows a density plot of the photon count intensity binned in the plane of event energy vs. event diffraction angle. In this space, photons which are due to XRF (e.g., due to contaminants in this case) appear as horizontal lines **205**, as shown, and photons due to XRD from crystallized regions with discrete atomic plane spacings (Miller indices) appear as arcs **210**, as shown, and trace out Bragg's law for n=1. After applying Bragg's law to compute d-spacing for individual photons, the XRD arcs **210** of FIG. **7***a* are straightened out as vertical lines **211** in FIG. **7***b*, while the horizontal XRF lines **205** of FIG. **7***a* remain as horizontal lines **206**. The XRD feature apparent at 1.73 Å is an instrument feature.

In each of FIGS. **7***a*-**7***b*, several of the XRD arcs **210** and vertical lines **211**, are labeled to show some of the expected (tabulated) and detected diffraction features due to aluminum, particularly showing the d-spacings of 1.22 Å, 1.44 Å, 2.04 Å, and 2.36 Å. These arcs **210** sweep from the upper left downwardly toward the lower right with increasing 2θ and represent constant d-spacing. From equations 2 and 14, it can be seen that the energy (E) of the events must decrease with increasing angle for a constant d-spacing. FIGS. **7***a*-**7***b* are also labeled to show the fluorescence features expected from trace elements in aluminum-6061 (e.g., Fe Kβ, Fe Kα, Cr Kβ, Cr Kα, Ti Kα). FIGS. **7***c*-**7***d* show how the event data can yield fluorescence (FIG. **7***c*) and diffraction (FIG. **7***d*) histograms. The diffraction histogram of FIG. **7***d* shows that the d-spacing arcs are of differing intensities. It can also be seen

that the d-spacing arcs in FIGS. **7***a* and **7***b* are broken up in intensity. This is due to a distribution of crystal grain size and planar orientations.

FIG. **7***e* is a three-color image of diffracted X-ray intensity, in angular coordinates, showing the result of extracting events from the three brightest d-spacing arcs for the aluminum sample in FIGS. **7***a*-**7***b* (i.e., the arcs corresponding to the d-spacings of 1.44 Å, 2.04 Å, and 2.36 Å), or equivalently the vertical features for the corresponding d-spacing values, and plotting the selected X-ray event locations on the CCD **120**, converted to angular coordinates representing the tip-tilt orientations of the crystallite planes. Given the selected d-spacing values and their tabulated correspondence to specific Miller indices (hkl), FIG. **7***e* depicts the orientations and sizes of crystallite lattice planes (hkl)=(**111**) (red), (**200**) (green), and (**220**) (blue). Thus, FIG. **7***e* shows the specular reflections off of crystal facets within the illuminated X-ray spot on the sample surface and the image can be analyzed to give detailed information about these facets, as well as gross distributions.

Example 2

Mineral Identification

FIG. **8** shows data from a bulk sample of hematite showing both diffraction and fluorescence features. As with FIG. **7***b*, the hematite data is binned and plotted in the space of energy (E) vs. d-spacing, as shown in FIG. **8**. XRD data is shown as vertical lines **221**, while the XRF data is shown as horizontal lines **225**. FIG. **8** is labeled to show some of the expected and detected diffraction features, particularly showing the d-spacings of 1.49 Å, 1.70 Å, 2.21 Å, 2.52 Å, and 2.70 Å. A faint d-spacing vertical line is also observable at 3.69 Å. FIG. **8** is also labeled to show the expected fluorescence features (e.g., Fe Kβ, Fe Kα, and Ti Kα).

Because d-spacing information acts as an effective "fingerprint" for any given mineral, the specific combination of vertical features **221** in FIG. **8** can be used to identify the sample. D-spacing values for thousands of organic and inorganic substances are available in commercial and freely available digital databases (e.g., www.webmineral.com), and the process of reducing data obtained by the XRD/XRF instrument **100** to identify minerals present in pure or mixed-phase samples lends itself to automation. Mineral identification algorithms based on matched filtering techniques are especially promising, as elemental composition from fluorescence reduces the number of tabulated minerals for which d-spacings must be matched to the sample.

"Rietveld refinement" (e.g., Bish & Howard 1988) of a one-dimensional diffractogram is the most common means of determining a sample's constituent minerals. The technique consists of fitting for the intensities and widths of diffraction peaks given expected crystal structures present in the sample. Although best suited to powders, the method allows for moderate preferred-orientation effects, which are likely in unprepared samples. The Rietveld treatment is least reliable when a small number of specular reflections contributes most of the flux in a diffraction peak, but in these instances the multi-wavelength approach of the XRD/XRF instrument **100** and techniques described herein allows measurement of the number, sizes, and orientations of the crystallites, quantities that are normally unknowns for which the Rietveld formulae attempt to find best-fit values as an intermediate step.

The use of the Rietveld technique as a tool for surface analysis of bulk samples is presently under study. It appears that the diffraction profile produced by an X-ray spot of about 1 mm in diameter illuminating a multi-phase, rocky sample is typically uncomplicated, with dominant d-spacings unique to just one or two minerals at a given position on the sample. Scanning the surface, or abrading it to expose sub-surface layers and collecting new X-ray data, then provides information about minor accompanying phases. It is therefore believed likely that a combination of Rietveld analysis, "bootstrapping" the dominant crystal phases, and judicious examination of bulk samples will readily reveal mineral content.

The high resolution d-spacing measurement resolution achievable with the XRD/XRF instrument **100** disclosed herein permits accurate mineral identification and enables the identification of different mineral phases within a sample.

Example 3

Aerosol Identification

Applications involving aerosols require a high detection limit to measure trace elements and require high sensitivity to permit analysis of minute amounts of material. A typical aerosol filter configured to collect particles on its surface (e.g., the Nuclepore® filter) holds about 20 μg/cm^2 of aerosol mass. For a X-ray beam **105** having a spot size area of about 2 mm^2, which is the case for the current example, the total aerosol mass observed by the beam is about 0.4 μg.

FIGS. **9***a*-**9***c* show an example of an aerosol filter, analyzed using the disclosed XRD/XRF instrument **100** and techniques disclosed herein, showing measurements of at least 9 elements with X-ray fluorescence and identifying at least three major minerals in the analyzed sample (i.e., calcite, hematite, and halite). The aforementioned second prototype of the XRD/XRF instrument **100** (see generally FIG. **2***b*) was used to analyze data from micrograms of dust collected on a thin polycarbonate Nuclepore® filter. Single-photon events detected by the CCD **120** are binned in energy (E) and d-spacing. Colors in FIG. **9***a* represent binned intensities as shown on the inset scale. Horizontal features **240** result from X-ray fluorescence and vertical features **241** result from X-ray diffraction, as previously noted. FIG. **9***a* shows, among other X-ray fluorescence features **240**, twelve measured or expected X-ray fluorescence features including Fe Kβ, Fe Kα, Mn Kα, Ti Kα, Ca Kβ, Ca Kα, K Kα, Ar Kα(air), S Kα, Cl Kα, P Kα, and Si Kα. The brightest XRF features have been excised from the data corresponding to FIG. **9***a* to form the d-spacing spectrum shown in FIG. **9***b*. FIG. **9***b* shows, for example, a Beryllium d-spacing at about 1.73 Å, due to the Beryllium window, calcite d-spacings at 2.10 Å, 2.28 Å and 3.04 Å, Hematite d-spacings at 2.51 Å and 2.69 Å, and a Halite d-spacing at 2.82 Å. FIG. **9***c* shows a photon energy spectrum for the data in FIG. **9***a*.

The outstanding sensitivity that allows for such analysis arise from the combination of the favorable geometry, the large detector cross section, the low noise/high sensitivity photon counting detector, and especially the simultaneous measurements at many different scattering angles, made possible by the use of a broadband X-ray source, provided by the XRD/XRF instrument **100** and techniques disclosed herein.

The aerosol analysis can be performed in several different modes. Three non-limiting modes are described below. First, filters may be collected in the field and saved for later analysis in a laboratory. Second, real-time or automated filter or impactation systems may be used to provide sampling and analysis directly in the field. For example, aerosol sampling and analysis can be performed automatically with the disclosed XRD/XRF instrument **100** and techniques in combination with another modality where the particles are sampled on a moving tape system that allows the sampled spot to move

in front of the XRD/XRF instrument window for analysis, such as is shown by way of example in FIG. **5***a*. Third, aerosol analysis may be performed in a real-time, "flyby" system where the aerosols (e.g., ice or other types of particles) are analyzed while still in suspension in the atmosphere, such as is shown by way of example in FIG. **5***b*. In this geometry, particles passing in the right geometry (i.e., a predefined volume about a known coordinate **125** (x_0, y_0, z_0)) in front of the window are flagged by a laser tagging system (e.g., laser scattering to a photodiode or photodiode array positioned in a geometry to see scattered photons coming from that particular volume). In at least some aspects, such predefined volume may comprise a volume of about $100\times100\times100\ \mu m^3$. In other aspects, the predefined volume may be larger or smaller.

Example 4

Volatiles Identification

Because the disclosed XRD/XRF instrument **100** and techniques do not require sample preparation, they can be used to analyze volatiles, such as water ice, which may evaporate if prepared for a conventional d-spacing XRD analysis. This particular aspect of the present concepts is particularly important for space exploration applications of the XRD/XRF instrument **100**, where powdering of water ice in a low pressure environment would cause the ice to evaporate and evidence thereof would be lost.

FIG. **10***a*-**10***c* show diffraction data for frost accumulated on the outside wall of a plastic receptacle containing liquid nitrogen. In FIG. **10***a*, known d-spacings from hexagonal ice (ice_h) and cubic ice (ice_c) (e.g., peaks for ice_h at 1.91 Å, 2.25 Å, 2.67 Å, 3.43 Å, 3.66 Å, and 3.88 Å and peaks for ice_c at 1.91 Å, 2.25 Å, 3.66 Å, and 3.88 Å) observed in a diffraction spectrum. The image in FIG. **10***b* shows the time-dependence of the observed d-spacings and maps changes in the diffraction peaks with time over a 15-minute interval. Up to six diffraction peaks are visible in a single 10-sec exposure, and there is evidence of a change at roughly the 10-minute mark wherein the diffraction peak at 2.25 Å grows stronger (i.e., darker or red to black in FIG. **10***b*) while a new peak at 3.66 Å begins to emerge. At the same time, the peaks at 2.07 Å and 2.67 Å appear to fade. Such analysis of rapidly time-dependent phenomena is virtually impossible with existing XRD instrumentation.

FIG. **10***c* shows a scatter-plot of individual photons distributed in angular diffraction coordinates, where color refers to different d-spacings of 1.91 Å (red), 2.25 Å (blue), 3.43 Å (deep sky blue), and 3.88 Å(magenta). FIG. **10***c* shows numerous distinct spots **250**, which are diffraction features (i.e., specular reflections), from frost grains of a few hundred microns in size. The spots **250** in FIG. **10***c* provide important texture data, which permits determination of the actual size of the frost grains causing the specular reflections based on the geometry of the XRD/XRF instrument **100** (e.g., the known angular relation between the X-ray source **110** and the photon-counting X-ray imaging spectrometer, such as CCD **120**)). This texture data, which also includes the location of the spot **250** (i.e., the tip-tilt of the frost grain) cannot be obtained from prepared samples, which destroys such crystalline texture data.

Example 5

Organic Crystal Identification

The disclosed XRD/XRF instrument **100** and techniques are also ideally suited for X-ray crystallography, the technique of choice for determining the molecular structures of organic compounds, including proteins that are vital for pharmacological studies. One simple organic crystal is common sugar, or sucrose.

The XRD/XRF instrument **100** and techniques disclosed herein provide novel benefits for crystallographic analysis. Traditional techniques for deriving crystal structure by inverting Laue patterns, collected without single-photon spectroscopy, are applicable to data obtained by the XRD/XRF instrument **100**, with the added enhancement that CCD **120** spectroscopy provides identifiable d-spacings for all observed Laue spots, even for a broad continuum energy band. Because the larger bandwidth samples previously unseen atomic plane orientation, the disclosed XRD/XRF instrument **100** can yield improved Laue inversions. Further, the high energy resolution of CCDs **120** should be sufficient to allow for new implementations of the "multi-wavelength anomalous dispersion" technique for solving the "phase problem" in deriving crystal structures.

FIGS. **11***a*-**11***b* display data for a single sugar crystal, roughly 200 microns on a side, obtained using the disclosed second prototype of the XRD/XRF instrument **100** over a period of about 3 hours. FIG. **11***a* shows a diffraction spectrum exhibiting known d-spacings of sucrose (e.g., peaks at about 1.45 Å, 1.87 Å, 2.35 Å, 2.68 Å, and 4.03 Å). FIG. **11***b* shows a diffraction pattern for the single-crystal of sucrose. In FIG. **11***b*, the diffraction pattern comprises Laue spots from distinct Miller indices corresponding to the color-coded d-spacings of 1.45 Å (red), 1.87 Å (blue), 2.35 Å (deep sky blue), 2.68 Å (magenta), and 4.03 Å (yellow).

In panel FIG. **11***a*, the sharp diffraction peaks for the d-spacings of 1.45 Å, 1.87 Å, 2.35 Å, 2.68 Å, and 4.03 Å sit on top of a much broader feature, which is due to scattering from largely amorphous Kapton, used as a membrane to hold the sugar crystal in the X-ray beam **105**. In FIG. **11***b*, it may be observed that streaks **260** arc clockwise from the two brightest Laue spots **265**. These streaks **260** are indications of misplaced charge. The misplaced charge arises in this prototype data because the specular reflections are bright enough that, as the CCD **120** reads out, photons continue to strike the detector, producing blurring along the readout direction. In future embodiments, these streaks may be minimized or eliminated by using CCDs with much faster readout times (e.g., less than about 1 second or, still better, less than 100 milliseconds) and/or frame-transfer regions. Alternatively, the X-ray source flux could be reduced in special cases where there are bright Laue spots.

The prototype data shown above in FIGS. **7***a*-**11***b*, together with the integration times necessary to achieve the evident signal-to-noise ratios, allow for robust estimates of the sensitivity that can be achieved by improving system components. Anticipated sensitivity gains through improvements in component technologies and systemic optimizations are discussed below. The total gain for the estimated improvements in sensitivity gain factor for further component and system improvements is expected to be about 10,000. It is noted that the aerosol data shown in FIGS. **9***a*-**9***c* required a 17-hour integration. It is estimated that future implementations of the present concepts implementing the following improvements will be able to replicate this dataset in a minute or less.

First, the deep-depletion CCD **120** for single photon X-ray spectroscopy may be improved by providing a larger collecting area, better energy resolution, higher quantum efficiency, a frame-store region, and a portable, low-noise readout. The larger collecting area provides a larger d-spacing range and/or increased sensitivity by collecting more of the Debye arcs (in continuum) for diffracted rays, producing an estimated sen-

sitivity gain factor of about 2.0. A better energy resolution would sharpen peaks in XRF and XRD spectra by about 50% to resolve closely-spaced features and boost S/N, producing an estimated sensitivity gain factor of about 1.2. A higher quantum efficiency broadens the range and resolution of XRD spectra, as well as the sensitivity to high-energy XRF lines (e.g., heavy metals in pollution aerosols) and is estimated to increase the sensitivity gain factor by about 1.2. The frame-store region would rapidly transfer charge from the illuminated CCD area, obviating need for a shutter and eliminating misplaced charge (small S/N gain) and is estimated to increase the sensitivity gain factor by about 1.1. The portable, low-noise readout is not estimated to increase the sensitivity gain factor, but will render thermo-electric cooling (TEC) sufficient, allowing for a lightweight field unit.

Improvements are also contemplated for the X-ray source **110** itself. By providing X-Ray Optical Systems (XOS® (of East Greenbush N.Y., USA)) polycapillary optics, it is possible to capture much larger solid angle of X-rays emitted by the source anode, significantly boosting flux relative to pinhole collimator, which flux is then guided to an aperture of chosen diameter. It is estimated that this improvement will alone increase the sensitivity gain factor by about 500, depending on the chosen aperture diameter. A higher beam current is further estimated to increase sensitivity gain factor by about 5 by increasing the continuum X-ray flux. A higher accelerating potential is also estimated to increase sensitivity gain factor by about 1.2 by increasing continuum X-ray flux, range of d-spacings, and likelihood of exciting XRF at higher energies. Still another improvement to boost the sensitivity gain factor includes alteration of the overall system geometry and vacuum windows to optimize CCD placement and window material. These improvements should broaden XRD range toward large d-spacings, increase sensitivity to XRF features below 2 keV, and reduce the aforementioned instrument features.

In the above-described XRD/XRF instrument **100** prototype data for the aerosol and frost samples, the aerosol and frost samples filled the X-ray beam **105**. This is the most efficient use of the available X-ray flux. For particles smaller than the beam, the sensitivity is reduced by the ratio of the areas of particle to beam. To mitigate this degradation, additional embodiments of our present concepts may advantageously utilize polycapillary optics, which will produce a net flux gain while focusing the X-rays to a chosen spot size (e.g., as small as 200 microns for parallel rays, or 10 microns in slightly converging rays) to allow for in-situ analysis of the smallest sample particles without intolerable loss of sensitivity. It may be conservatively estimated that a 200-micron beam on a 10-micron particle will result in an overall sensitivity gain of a factor of 20. For the smallest particles, there will also be a loss term due to transmission through the particle without an XRF or XRD interaction. At the photon energies that will often be employed in combination with the disclosed XRD/XRF instrument **100**, this loss term will amount to a factor of 2 loss, so that the net sensitivity gain is still an order of magnitude (i.e., a gain of 10). With the frost data discussed above in relation to FIGS. **10***a*-**10***c*, six d-spacing XRD features were detected in a single 10-sec frame. Given the factor of 10 sensitivity boost, a high-sensitivity XRD/XRF instrument **100** should allow this same level of statistical significance for a single 10-micron ice crystal in the same time or less.

Although the combined use of (1) a continuous spectrum of X-rays, and (2) the geometry of reflection, instead of transmission, is discussed herein in relation to certain of the embodiments and aspects disclosed herein, together with attendant benefits flowing therefrom with respect to the disclosed XRD/XRF instrument **100** and the disclosed methods or acts, the disclosed XRD/XRF instrument **100** as well as the disclosed methods or acts may be utilized in combination with a transmissive geometry and/or a prepared sample. For example, certain of the disclosed XRD/XRF instrument **100**, methods, or acts, to the extent not logically prohibited, may use a thin sample, prepared or unprepared (e.g., single crystal), and transmit an X-ray beam (e.g., **105**) from the X-ray source (e.g., **110**) through the thin sample. FIGS. **12***a*-**15***b*, discussed below, schematically show the types of data that would result from four potential combinations of instrument type (single-wavelength in FIGS. **12***a*-**12***b* and **14***a*-**14***b*, multi-wavelength in FIGS. **13***a*-**13***b* and **15***a*-**15***b*) and sample preparation (powdered in FIGS. **12***a*-**12***b* and **13***a*-**13***b*, unprepared in FIGS. **14***a*-**14***b* and **15***a*-**15***b*). In other words, the series of plots represented in FIGS. **12***a*-**12***b* through **15***a*-**15***b* show a comparison of the characteristics of some types of data obtained using an XRD/XRF instrument **100** in accord with the present concepts and the data obtainable using other XRD/XRF instruments **10**, such as that shown in FIG. **1**, under the same conditions.

FIGS. **12***a* and **13***a* show schematically in a CCD Y-position vs. X-position plot the types of data that would result from the XRD/XRF instruments **32**, **100** (i.e., single-wavelength vs. broad spectrum, respectively) for a powdered sample. FIGS. **12***b* and **13***b* show schematically in an energy vs. X-position plot the types of data that would result from the XRD/XRF instruments **32**, **100** (i.e., single-wavelength vs. multi-wavelength, respectively) for a powdered sample.

FIG. **12***a* shows the traditional configuration for X-ray diffractometry wherein a single-wavelength XRD/XRF instrument **32** is used on a powdered sample. The addition of an energy-dispersive detector, such as CCD **46** shown in FIG. **1**, allows for simultaneous fluorescence spectroscopy, but with potentially poor efficiency because of the potential for mismatches between the single input X-ray energy and the characteristic lines of elements in the sample. Diffracted X-rays striking the CCD **46** form arcs **505**, **510** in the image (X-Y) plane. These arcs **505**, **510**, known as Debye rings, arise because the orientations of crystal grains ("crystallites") in the sample have been randomized by the powdering of the sample. However, the powdered sample lacks texture (i.e., a non-random distribution of crystallographic orientations of a sample) since the processing of the sample for XRD/XRF analysis seeks to eliminate any preferred orientation of the crystallites. Thus, valuable texture information, which can be an important factor in understanding the mechanical, physical and/or chemical behavior of the sample, is lost.

FIG. **12***b* shows the registering of event energies on CCD **46** in the form of a scatter plot of energy (E) vs. X-position. Specifically, FIG. **12***b* shows X-rays emitted through fluorescence as horizontal lines **515**, **520**, while the diffraction arcs **505**, **510** in FIG. **12***a* are shown to collapse to short segments **525**, **530** in X at the fixed energy of the X-ray source. The distribution of the horizontal fluorescence lines **515**, **520**, is essentially independent of position.

FIGS. **13***a*-**13***b* represent plots for a configuration wherein the broad spectrum XRD/XRF instrument **100** in accord with aspects of the present concepts outputs a continuum spectrum of X-rays onto a powdered sample. In FIG. **13***a*, fluorescence of the sample produces X-rays that are distributed isotropically (i.e., directionally invariant) over the detector (e.g., CCD(s) **120**), while diffracted rays strike the detector at a wavelength (λ) and angle (θ) satisfying Bragg's law. Because the X-ray source produces a continuum spectrum of wavelengths, and the powdered sample contains a continuum of

crystallite orientations that determine θ, the resulting distribution of diffracted photons on the imaging surface of the CCD(s) **120** is also virtually isotropic, resulting in a generally featureless image. In the energy (E) vs. X-position plot of FIG. **13***b*, the diffraction events forming arcs **540**, **545** reflect individual d-spacings of the sample, consistent with Bragg's law. Individual arcs arising from distinct d-spacings can be resolved as permitted by the energy resolution and spatial resolution capability of the CCD(s) **120** As in FIG. **12***b*, fluorescence events in FIG. **13***b* appear as horizontal lines.

FIGS. **14***a* and **15***a* show schematically in a CCD Y-position vs. X-position plot the types of data that would result from the XRD/XRF instruments **32**, **100** (i.e., single-wavelength vs. broad spectrum, respectively) for an unprepared sample. FIGS. **14***b* and **15***b* show schematically in an energy vs. X-position plot the types of data that would result from the XRD/XRF instruments **32**, **100** (i.e., single-wavelength vs. broad spectrum, respectively) for an unprepared sample.

FIG. **14***a* shows a representation of a CCD Y-position vs. X-position plot for a conventional single-wavelength XRD/XRF instrument **32** (see, e.g., FIG. **1**) used on an unprepared sample. This is the worst-case scenario for traditional XRD studies. Unlike powdered samples, the orientations of crystallites in an unprepared sample are potentially highly-aligned or, in a pure single crystal, strictly aligned. Thus, diffracted rays may be preferentially oriented in a single direction. If the detector (e.g., CCD **46** of FIG. **1**) does not cover a sufficient solid angle to intercept the diffracted ray, that ray will be missed, resulting in the loss of valuable d-spacing information. For this reason, traditional diffractometers **32** are designed so that the detector is mounted on a movable stage (or, equivalently, the sample is placed on a rotating holder, a goniometer). As previously noted, these moving parts reduce the reliability of the device and substantially increase the time it takes to acquire data at many angles, which is required for crystallographic studies. If some crystallites are fortuitously aligned with a stationary detector, some diffracted flux will be measured in certain locations, producing "splotches" **601**, **602** along the same arcs that would have resulted from a powdered sample. In FIG. **14***a*, the dashed curves **604**, **606** represent these undetected arcs. FIG. **14***b* shows fluorescence events as horizontal lines **612**, **614**. FIG. **14***b* also shows that any X-rays producing "splotches" **601**, **602** would appear as points or short segments **607**, **609** in X at the fixed energy of the X-ray source.

FIG. **15***a* shows a representation of the use of the broad spectrum XRD/XRF instrument **100** in accord with aspects of the present concepts on an unprepared sample. Because the X-ray source (e.g., **110** in FIG. **2***b*) outputs a range of X-ray wavelengths, diffracted X-rays satisfying Bragg's law (shown as different shades of gray in FIGS. **15***a*-**15***b* for different d-spacings) from pure crystals are virtually guaranteed to strike the stationary detector (e.g., CCD **120** in FIG. **2***b*). In the image plane (Y-X plane) of FIG. **15***a*, one or more splotches **650**, **660** will appear depending on the ratio of crystallite size to the size of the illuminated X-ray beam **105** spot on the sample surface. If many small crystallites of a given d-spacing and having arbitrary orientation are illuminated, their diffracted outgoing X-rays will produce a pattern of splotches **650**, **660** through specular reflection that contains valuable information about the crystalline texture. In the E-X plane, the events corresponding to the splotches **650**, **660** are constrained by Bragg's law to lie on constant d-spacing arcs **655**, **665**, while fluorescence lines **670**, **680** are again distinguished because their energies do not depend on event position on the CCD **120**.

The use of a continuous spectrum of X-rays in combination with a geometry of reflection, instead of transmission, provides at least some of the benefits described herein. For example, although both the broad spectrum XRD/XRF instrument **100** (see generally FIGS. **2***a*-**15***b*) and the conventional XRD/XRF instrument **32** both detect diffracted X-rays from forward-scattered cones emanating from the sample, the broad spectrum XRD/XRF instrument **100** typically examines the sample in a reflection geometry, while the conventional XRD/XRF instrument **32** requires, without exception, transmission of X-rays through the sample. Two immediate consequences follow. Because X-rays of a few keV in energy penetrate only tens of microns in typical minerals, this determines the maximum thickness of a sample and correspondingly requires the need to grind up the sample into a powder of sufficient fineness to permit transmission of X-rays through the sample. Unfortunately, such handling destroys valuable information originally contained in the sample about crystal grain sizes and the orientations of their lattice planes while also releasing volatiles, such as water ice. In a reflection geometry, the low transmission depth means that the analysis is necessarily of surface material, but this is not a disadvantage. Once the surface has been examined, an abrasion tool can be used to remove surface layers and explore within. In each case, the crystal grains and volatiles in the sample remain largely undisturbed.

Further, as previously noted, the transmission configuration of the XRD/XRF instrument **32** in FIG. **1** requires sample material to be transported inside the instrument, resulting in significant mechanical complexity, increased risk of failure or contamination (e.g., of the CCD, or in cross-sample residual powder), and the inability to analyze bulk samples. In the disclosed embodiments of the XRD/XRF instrument **100** utilizing a reflection geometry, the option is available to seal the instrument's sensitive components to prevent direct contact with the sample and, instead of transporting the sample inside the XRD/XRF instrument, the instrument can simply be placed against any surface to obtain comprehensive XRD/XRF analysis.

Still other advantages stem from the disclosed XRD/XRF instrument **100**'s unique use of continuum spectrum X-rays and the spectroscopic capability of the CCD **120**, not only to provide XRF spectra, but to detect the characteristic spatial patterns of diffracted X-rays as well. The disclosed XRD/XRF instrument **100** X-ray source **110** provides an emission spectrum dominated by continuum. For samples containing large, well-ordered crystal grains, diffraction will produce specular reflections of X-rays according to Bragg's law, instead of smooth Debye arcs, and the spatial pattern imaged by the CCD will consist of a number of bright spots. With a fixed detector and limited imaging area, the range of angles sampled in both 2θ and azimuth (i.e., along a Debye arc) is constrained. With monochromatic X-rays, such as with the conventional XRD/XRF instrument **32**, the coverage provided by the detector's collecting area limits the range of d-spacings that can be sampled, no matter the orientations of crystal grains in the sample. Worse, for highly organized crystal samples, diffraction peaks may be altogether absent for unfavorable orientations of the lattice planes (e.g., Bragg's law fixes the relationship between d-spacing, the diffracted angle, and the wavelength, resulting in constructive interference from only those crystallites satisfying a particular orientation). The conventional XRD/XRF instrument **32** remedies this situation by powdering the sample to randomize the orientations of the crystal grains and improve the chances that some diffracted rays will strike the detector. However, the improved XRD/XRF instrument **100** and techniques dis-

closed herein using a range of input X-ray wavelengths provides sensitivity to a much broader range of d-spacings by allowing λ in Bragg's law to vary and by permitting sampling by the detector **120** of a range of 2θ information. Similarly, preferred-orientation effects are minimized, as the chances of a diffraction peak at some wavelength striking the detector are significantly improved. The disclosed XRD/XRF instrument **100** and techniques therefore take full advantage of a CCD's **120** collecting area and spectroscopic capability.

It is noted that, to achieve sufficient angular coverage in a transmission geometry using a monochromatic X-ray beam, such as is used in CheMin, the sample material must be placed very close (a few mm) to the CCD **46**. In addition to increased mechanical complexity and risk to the CCD, this geometry requires that the X-ray spot illuminating the sample be very small, about 50 microns. As a result, a highly focused X-ray source would be a fundamental requirement for such conventional XRD/XRF instrument **32**. With the disclosed XRD/XRF instrument **100**, the sample can be placed 2-3 cm away from the CCD **120** for comparable XRD performance, resulting in looser tolerances on the X-ray source **110** while also allowing a much higher X-ray flux to illuminate the sample. The disclosed XRD/XRF instrument **100** is therefore a faster instrument, providing the same XRD information in much less time than the conventional XRD/XRF instrument **32** given the same X-ray source power.

Further, the use of a broad continuum spectrum of X-rays to illuminate a sample **126** in the disclosed XRD/XRF instrument **100** results in a faster XRF instrument for the reason that atoms fluoresce most efficiently when they are excited by radiation that closely matches their electron-shell transition energies. Monochromatic photons, such as those utilized in the conventional XRD/XRF instrument, cannot efficiently excite transitions in a wide variety of elements. In contrast, in aspects of the disclosed XRD/XRF instrument's **100** having a continuum emission up to about 10-15 keV a good match for all but the highest-Z elements is assured.

FIG. **16** compares the expected d-spacing measurement resolution (full width at half-maximum of diffractogram peaks) of the disclosed third prototype XRD/XRF instrument **100** (see, e.g., FIG. **2***c*) to the XRD/XRF instrument **32** (i.e., a monochromatic, transmission-based geometry XRD instrument such as CheMin) shown in FIG. **1**. The d-spacing measurement resolution curve of the XRD/XRF instrument **32** for a constant $\delta(2\theta)=0.3°$ is represented by reference numeral **750**. For the disclosed XRD/XRF instrument **100**, FIG. **16** shows the results for four representative photon energies (1.5 keV (curves **710***d*, **720***d*, and **730***d*), 2.5 keV (curves **710***c*, **720***c*, and **730***c*), 6 keV (curves **710***b*, **720***b*, and **730***b*), and 9 keV (curves **710***a*, **720***a*, and **730***a*), including the anticipated contributions of geometric smearing and energy resolution for such photon energies. Specifically, curves for the geometric smearing term ($\delta\theta$ terms) are shown as **710***d* (1.5 keV), **710***c* (2.5 keV), **710***b* (6 keV), and **710***a* (9 keV). The curves for the energy resolution (a terms) are shown as **730***d* (1.5 keV), **730***c* (2.5 keV), **730***b* (6 keV), and **730***a* (9 keV). The geometric term is the result of the expected collimation of the X-ray beam **105** to a 0.5 mm diameter and the attendant spot size on the sample, where photons originating from a non-zero extent in sample position (x_0,y_0,z_0) may strike the same detector pixel, blurring the inferred **28**, and thence d-spacing, values. The energy-resolution term enters into the d-spacing measurement directly through the conversion of energy to wavelength and its application in Bragg's law. Where the highest possible d-spacing resolution is needed, an X-ray source outputting characteristic emission lines may be used so that the detector's energy resolution is not a limiting factor.

In FIG. **16**, it is assumed that the sample fills the 0.5 mm diameter beam X-ray beam. At small d-spacing values, the performance of the disclosed third prototype XRD/XRF instrument **100** (see, e.g., FIG. **2***c*) is comparable to the XRD/XRF instrument **32**. However, at larger d-spacing values, the disclosed third prototype XRD/XRF instrument **100** outperforms the XRD/XRF instrument **32**. High resolution in measuring d-spacing is essential for accurate mineral identifications and for distinguishing mineral phases within a sample. For samples smaller than the 0.5 mm beam diameter assumed here, the geometric contributions (dotted curves in FIG. **16**) to the error budget are much reduced, so that the XRD/XRF instrument **100** resolution is improved, especially at small d-spacing values.

FIGS. **17***a*-**17***b* depict a dual geometry XRD/XRF instrument **600** in accord with at least some aspects of the present concepts, the instrument comprising an X-ray source **610** and a movable CCD vacuum chamber **615** comprising a CCD **620**. In the present example, the X-ray source **610** comprises either X-ray polycapillary optics and/or a collimator in a vacuum enclosure. A Beryllium window (not shown) is provided at an output end of the X-ray source **610**. The movable CCD vacuum chamber **615** includes, as illustrated, two windows, a first window **630** and a second window **640**. Alternatively, a single window, or more than two windows may be provided. The first window **630** is disposed parallel to the array of CCD **620**, whereas the second window **640** is disposed at an angle to the array of CCD **620**. When the CCD vacuum chamber **615** is disposed in a first position, as shown in FIG. **17***a*, the first window **630** is disposed to provide, relative to the X-ray source **610**, a transmission geometry. When the CCD vacuum chamber **615** is disposed in a second position, as shown in FIG. **17***b*, the second window **640** is disposed to provide, relative to the X-ray source **610**, a reflection geometry.

In the example of FIGS. **17***a*-**17***b*, the CCD vacuum chamber **615** is disposed to travel within an arcuate track **616**. Alternative mechanisms may also be provided to permit translation and/or rotation of the dual geometry XRD/XRF instrument **600** components relative to one another to permit transition between a transmissive geometry and a reflective geometry. In some aspects, rotation of the CCD vacuum chamber **615** within the track **616** causes a corresponding rotation or movement of the sample support **625**. In other aspects, the sample support **625** is fixed.

Aspects of one method in accord with the present concepts, as well as some noted optional variations thereon, is provided below. The acts in the example presented are illustrative, but may be executed in combination with additional non-enumerated acts or in an order other than that presented, to the extent permitted by the data available at any particular juncture.

In an act **A110** according to a method for performing X-ray diffraction and X-ray fluorescence in accord with at least some aspects of the present concepts, single-photon events are extracted from the CCD **120** images, producing best estimates of X and Y coordinates, photon energy, and recording start and/or stop time of the exposure. The extraction is done by first subtracting a "dark frame" image, a readout of the pixel contents when the CCD **120** is not illuminated by any radiation, and then systematically searching for local maxima in the resulting background-subtracted image. The digitized values read out for each pixel represent accumulated electric charge, which is proportional to the energy of the photon striking the pixel. The simplest search for localized bright pixels consists of a threshold set sufficiently high so as to avoid fluctuations in the recorded charge due to noise (as recorded, e.g., in the dark frame). A more sophisticated search

allows for the possibility that charge deposited by an ionizing photon is distributed into two or more pixels in a tight cluster (e.g., a 3×3 pixel "island"), where a second threshold value may be applied to determine whether an adjacent pixel's brightness is sufficiently high so as to warrant its inclusion in the estimate of total deposited charge for that photon.

The search process then returns X, Y of each pixel (or center of 3×3 island) above threshold, together with the total charge (from a single pixel or summed over the island) and frame readout time. The search process can optionally provide event morphology data for each of these events by describing the distribution of split charge either as a total number of split charge pixels detected per local maximum above threshold or as an encoded expression. The event morphology is used to reject events generated by cosmic rays which is important for space applications. It is also used to optimize the detection efficiency of X-ray photons while maximizing the energy resolution. At this point a selection criterion can be used to only accept events with a given morphology (e.g., single-split or non split events). This basically follows event processing algorithms discussed in Gendreau, K. C., PhD Thesis MIT (1995). From this point forward, the morphology information can be ignored. The result is a filtered event list of X, Y, total charge (energy), and frame readout time. Optionally, it may also be advantageous to accumulate a one-dimensional histogram of energy values as an XRF spectrum to calibrate the detector's gain.

In an act A**120**, total charge is converted to photon energy. The proportionality relationship, or gain, that links charge to photon energy must be calibrated for any given CCD **120** or other detector. This calibration is typically stable for days or weeks, or longer, provided that the detector's nominal operating temperature is maintained. Gain values may be derived by acquiring data on a calibrator sample (e.g., any substance exhibiting fluorescence lines that span a range of energies, such as Ti Kα through Fe Kβ or others, as seen in the Al 6061 data example, above), or, if the XRD/XRF sample **126** has useful lines, the data may be self-calibrated. In an act A**122**, a one-dimensional histogram of photon energies is accumulated for detector calibration through the identification of XRF features.

At this point, XRF analysis is possible, but the presence of XRD photons in the dataset may degrade the quality of XRF spectra unless at least some of the following acts are taken.

In an act A**130**, the photon energy for each photon is converted to wavelength using (Eq. 14)(i.e., λ=hc/E), as described above.

In an act A**140**, for a given instrument, the sample position (x0,y0,z0) and incoming beam angle θγ must be measured or calibrated as already described (i.e., either by optical measurement or by using a calibrator sample, such as aluminum). The fixed parameters (θγ, its intercept with the z axis, and y0) apply to all subsequent datasets. One free parameter remains, position along the incoming X-ray beam **105** line, that can be adjusted from sample to sample.

In an act A**150**, X and Y coordinates for each photon are converted to diffraction angles (θ, ϕ) for each photon, following geometry already described, assuming the nominal values of calibrated sample position described above or some other position values. Depending on the instrument geometry and detector size and shape, the curvature of the segments of diffraction cones intercepted by the XRD/XRF instrument **100** detector (e.g., CCD **120**) may be very small, in which case photon Y information is not especially valuable, and X alone can be used to estimate θ.

In an act A**160**, using Bragg's law (Eq. 2), a d-spacing value is computed for each detected photon given the wavelength λ determined in act A**130**, above, and θ from act A**150**, above. At this point, XRD analysis is possible, but the presence of XRF photons in the dataset may potentially degrade the quality of XRD spectra unless some of the following optional acts are taken. For example, depending on the intended application, an optional act may include accumulating a two-dimensional image binned in energy (E) vs. 2θ. Another optional act A**164** may include accumulating a two-dimensional image binned in E vs. d-spacing value. In this way XRF features would be orthogonal to XRD features which may be useful in filtering of the data.

An act A**166** includes accumulating a one-dimensional histogram of d-spacing values for instrument calibration. If sample surface roughness or imprecise placement result in inconsistency between the sample's actual position and the assumed, calibrated position (i.e., adjustment of the remaining free parameter in positioning is needed), the d-spacing resolution will be degraded. This may be diagnosed, in act A**168**, through not-quite-vertical features in an energy vs. d-spacing image, or equivalently in broad diffractogram peaks. The diagnosis may be performed in at least one aspect by an automated search for the correct position performed by "peaking up" the diffractogram by repeating acts A**150**, A**160**, A**164**, and/or A**166**, until the widths of the diffractogram peaks are minimized and/or their intensities have been maximized. For samples with strong preferred orientation effects, however, this technique may not be applicable.

Once the location of the illuminated spot on the sample has been ascertained and d-spacing values computed for all photons, the act(s) of accumulating a two-dimensional image binned in energy (E) vs. 2θ and/or accumulating a two-dimensional image binned in E vs. d-spacing value are repeated. XRD and XRF phenomena in the dataset may be separated, as demanded by the data, by applying one or more of the techniques already described, such as but not limited to, filtering of horizontal and vertical features in images created in act A**164**, 2-D Fourier filtering of images created in the acts of accumulating a two-dimensional image binned in energy (E) vs. 2θ and/or accumulating a two-dimensional image binned in E vs. d-spacing value, and/or 2-D simultaneous fitting of XRD and XRF features by matched filtering.

Additionally, following the aforementioned filtering, the method may optionally include accumulating a one-dimensional histogram of d-spacing values for traditional XRD analysis and/or accumulating a one-dimensional histogram of photon energies for traditional XRF analysis. Such histogram should be normalized to account for variations in energy bandwidth and detector area for each of the d-spacing bins into which the histogram is accumulated.

Still further, the method may include, in an act A**180**, filtering of photon events for one or more d-spacing values, accumulating images in either (X,Y) or (θ, ϕ) for crystal texture analysis. Features associated with each d-spacing may be plotted in a different color and the individual images combined into a single multi-color image to highlight the relative locations and orientations of the different atomic planes represented by the d-spacing values.

Optionally, additional acts may include generation of analysis products that combine, in various ways, two- or three-dimensional subsets of the four-dimensional data space. For example, time variability of d-spacings may be displayed as an accumulated image, such as is shown by in relation to the example of FIGS. **10**a-**10**c, or similarly for time-varying XRF spectra. Another example would be to create a movie of time-dependent crystal texture by combin-

ing texture images, such as that provided by way of example in FIG. **10***b*, formed for data accumulated in subsets of the full exposure.

The flow chart in FIG. **18** shows one aspect of the data analysis method disclosed above following collection of the XRD/XRDF data in the imaging spectrometer device. The depicted aspect may be used in combination with other intermediate acts, described above.

Each of these embodiments and obvious variations thereof is contemplated as falling within the spirit and scope of the claimed invention, which is set forth in the following claims. As one example, the disclosed XRD/XRF instruments (e.g., **100**, **600**) may also advantageously comprise a grid (i.e., a reticule) provided between the sample (e.g., **126**) and detector (e.g., CCD **120**) to enable reticulography. Such grid may, for example, be incorporated into the window **145***b*. The grid comprises a X-ray absorbing material (e.g., a metal) so that the reticule produces dark lines or shadows in the resulting image. The shadows cast by the grid lines facilitate interpretation of the pattern of spots and splotches (see, e.g., **650**, **660** in FIG. **15***b*) that get reflected from a polycrystalline sample onto the detector. As one additional example, although the present concepts are described in many examples in relation to unprepared samples, there are many applications where prepared or treated samples are highly desirable and the present concepts expressly include utilization of prepared samples in either the reflection geometry or transmission geometry. In still additional alternative embodiments, the present concepts may comprise optical spectroscopy, wherein additional lenses or mirrors, plus an optical diffraction grating, could be added to the system in order to allow the same (X-ray) CCD or a second one to perform the optical reflectance spectral analysis of the sample. Alternatively, a fiber optics spectrometer could be coupled to the system simultaneously observing the sample volume. Still further, the XRD/XRF instrument **100** may comprise a mechanism by which the X-ray beam spot size may be selectively altered to shrink or expand the X-ray beam spot size (e.g., by providing a plurality of selectable collimators, lenses, etc.).

What is claimed is:

1. An X-ray diffraction and X-ray fluorescence instrument for analyzing samples having no sample preparation, comprising:

- a X-ray source configured to output a collimated X-ray beam comprising a continuum spectrum of X-rays to a predetermined coordinate;
- a photon-counting X-ray imaging spectrometer disposed to receive X-ray photons output from an unprepared sample disposed at the predetermined coordinate upon exposure of the unprepared sample to said collimated X-ray beam; and
- a housing defining a vacuum chamber and a sample aperture, the sample aperture comprising an X-ray window disposed therein,
- wherein the X-ray source and the photon-counting X-ray imaging spectrometer are arranged in a reflection geometry relative to the predetermined coordinate,
- wherein the X-ray source is disposed in the vacuum chamber at a first side of the housing and the photon-counting X-ray imaging spectrometer is disposed at a second side of the housing in the vacuum chamber or in another vacuum chamber at the second side of the housing,
- wherein said predetermined coordinate is adjacent an exterior of the X-ray window, and
- wherein said sample aperture comprises a first X-ray window disposed between said X-ray source and said predetermined coordinate outside of the housing and a second X-ray window disposed between said predetermined coordinate outside of the housing and said photon-counting X-ray imaging spectrometer.

2. An X-ray diffraction and X-ray fluorescence instrument according to claim **1**, wherein said first X-ray window is inclined to a position substantially perpendicular to said collimated X-ray beam and wherein said second X-ray window is inclined to a position substantially parallel to said photon-counting X-ray imaging spectrometer.

3. An X-ray diffraction and X-ray fluorescence instrument according to claim **2**, further comprising:

- an optical lens disposed in said sample aperture;
- an optical charge coupled device disposed within said housing opposite to said optical lens; and
- a partition dividing said housing into a first vacuum chamber and a second vacuum chamber, the X-ray source, optical charge coupled device, and first X-ray window being disposed in said first vacuum chamber and said photon-counting X-ray imaging spectrometer and second X-ray window being disposed in said second vacuum chamber.

4. An X-ray diffraction and X-ray fluorescence instrument according to claim **2**, further comprising:

- an optical lens disposed in said sample aperture;
- a movable shutter configured to selectively open and close to respectively transmit or block light output by said optical lens; and
- a mirrored surface disposed to receive light output from said optical lens and to reflect said light onto said photon-counting X-ray imaging spectrometer.

5. An X-ray diffraction and X-ray fluorescence instrument for analyzing samples having no sample preparation, comprising:

- a X-ray source configured to output a collimated X-ray beam comprising a continuum spectrum of X-rays to a predetermined coordinate;
- a photon-counting X-ray imaging spectrometer disposed to receive X-ray photons output from an unprepared sample disposed at the predetermined coordinate upon exposure of the unprepared sample to said collimated X-ray beam;
- a housing defining a vacuum chamber and a sample aperture, the sample aperture comprising an X-ray window disposed therein; and
- an aerosol delivery system, the aerosol delivery system comprising a plurality of aerosol collection spots disposed on a movable substrate, a movable substrate, and a drive system configured to selectively move the aerosol collection spots to said predetermined coordinate,
- wherein the X-ray source and the photon-counting X-ray imaging spectrometer are arranged in a reflection geometry relative to the predetermined coordinate,
- wherein the X-ray source is disposed in the vacuum chamber at a first side of the housing and the photon-counting X-ray imaging spectrometer is disposed in the vacuum chamber at a second side of the housing or in another vacuum chamber at the second side of the housing, and
- wherein said predetermined coordinate is adjacent an exterior of the X-ray window.

6. A method for performing X-ray diffraction and X-ray fluorescence on an unprepared sample, the method comprising the acts of:

- placing an unprepared sample at a predetermined coordinate position of an X-ray diffraction and X-ray fluorescence instrument comprising a broad-spectrum X-ray source and a photon-counting X-ray imaging spectrom-

eter arranged in either a reflection geometry or a transmissive geometry relative to the predetermined coordinate position;

outputting from the broad-spectrum X-ray source a collimated X-ray beam comprising a continuum spectrum of X-rays to the sample;

receiving, at the photon-counting X-ray imaging spectrometer, X-ray photons output from the sample upon exposure of the sample to the collimated X-ray beam;

outputting to a processor data corresponding to each X-ray photon registered by said photon-counting X-ray imaging spectrometer;

preparing an event list; and

analyzing, using the event list, at least one of a crystalline texture, crystalline topography, grain size, particle size, or time dependence of crystalline structure of the unprepared sample.

7. A method for performing X-ray diffraction and X-ray fluorescence according to claim **6**, wherein the event list comprises an energy of an incident photon and an X-position, a Y-position, or both an X-position and a Y-position at which the incident photon is received by the photon-counting X-ray imaging spectrometer.

8. A method for performing X-ray diffraction and X-ray fluorescence according to claim **7**, wherein the event list comprises time.

9. A method for performing X-ray diffraction and X-ray fluorescence according to claim **7**, the method further comprising the acts of:

converting X-position and Y-position data to diffraction angle θ and cone azimuth ϕ for each X-ray photon event sensed by said photon-counting X-ray imaging spectrometer.

10. A method for performing X-ray diffraction and X-ray fluorescence according to claim **9**, the method further comprising the act of:

converting event energy to wavelength for each X-ray photon event sensed by said photon-counting X-ray imaging spectrometer.

11. A method for performing X-ray diffraction and X-ray fluorescence according to claim **10**, the method further comprising the act of:

calculating the d-spacing for each event.

12. A method for performing X-ray diffraction and X-ray fluorescence according to claim **11**, the method further comprising the act of:

plotting the event data in the space of energy versus d-spacing so that X-ray diffraction and X-ray fluorescence features of interest are orthogonal.

13. A method for performing X-ray diffraction and X-ray fluorescence according to claim **12**, the method further comprising the acts of:

filtering event data from the event list to provide data for X-ray photons consistent with diffraction from a single d-spacing, and

imaging the size and orientation distributions for crystal grains containing said single d-spacing.

14. A method for performing X-ray diffraction and X-ray fluorescence according to claim **6**, wherein said time dependence of crystalline structure comprises time dependence of at least one of crystalline texture, crystalline topography, grain size, particle size, d-spacing values, relative diffraction intensities, relative fluorescence intensities, crystal growth, or crystal degradation.

15. An X-ray diffraction and X-ray fluorescence instrument for analyzing an unprepared sample, comprising:

a X-ray source configured to output a collimated X-ray beam comprising a continuum spectrum of X-rays to a predetermined coordinate;

a photon-counting X-ray imaging spectrometer disposed to receive X-rays output from an unprepared sample disposed at the predetermined coordinate upon exposure of the unprepared sample to the collimated X-ray beam, the X-ray source and the photon-counting X-ray imaging spectrometer being arranged in either a reflection geometry or a transmission geometry relative to the predetermined coordinate;

a processor; and

a computer-readable medium bearing instructions configured to cause the processor to carry out the steps of preparing an event list from information output to the processor by said photon-counting X-ray imaging spectrometer and analyzing, using the event list, at least one of a crystalline texture, crystalline topography, grain size, particle size, or time dependence of crystalline structure of the unprepared sample.

* * * * *